

Particles Composition and Interactions Using the Nuon Model

René Brun

CERN, Geneva, Switzerland

Email: rene.brun@cern.ch

How to cite this paper: Brun, R. (2023) Particles Composition and Interactions Using the Nuon Model. *Journal of Modern Physics*, 14, 623-665.
<https://doi.org/10.4236/jmp.2023.145036>

Received: February 7, 2023

Accepted: April 18, 2023

Published: April 21, 2023

Copyright © 2023 by author(s) and Scientific Research Publishing Inc.

This work is licensed under the Creative Commons Attribution-NonCommercial International License (CC BY-NC 4.0).

<http://creativecommons.org/licenses/by-nc/4.0/>



Open Access

Abstract

The Standard Model in Particle Physics has been able to make many predictions confirmed later with a flow of experimental results. With the discovery of the Higgs boson at the LHC, one is full of admiration for the people contributing to this model fifty years ago and its predictions that have been confirmed gradually. The original particle quark constituent model has evolved with the deep inelastic experiments to a quark and gluons system, then to a more general system with virtual quarks. This work is the result of observations while working at CERN in Geneva with many different experiments at the ISR, SPS, LEP, LHC colliders. A new model based on nuons is introduced, that allows accurate evaluations of the particle masses (mesons and baryons) and magnetic moment, computes very accurately the kinematics distributions for particles and jets observed in the p-p collisions at the LHC (elastic and inelastic) and at lower energy machines. This new model looks at a first glance in contradiction with the quark model because it can build the elementary particles with nuons only, *i.e.* electrons and neutrinos. However, all the existing physics involved in electron, positron and neutrino interactions may be used to explain interactions between composite particles such as protons or heavy ions.

Keywords

Standard Model, Particle Masses, Particles Interactions, Elastic Scattering, Deep Inelastic, Jets, Charge Density

1. Introduction: Motivation and Ideas

The Standard Model (SM) [1]-[8] has been successful in describing particle interactions since its introduction in the late sixties. Many predictions have found their confirmations in the past 3 or 4 decades. The search for the Higgs boson

and its properties is the best proof of confidence of the vast majority of physicists for its predictions.

I have started my career as a nuclear physicist at a time where the Standard Model was shaping-up, then I spent all my professional career as an applied physicist developing general tools for the simulation of detectors, e.g. GEANT [9], or data analysis tools such as PAW [10] and ROOT [11]. Thanks to these tools I have been in contact with very many experiments in the world of High Energy or Nuclear Physics in the past four decades. During these developments, I have always been very interested by the research topics of these experiments and I had the unique opportunity to have a very good overview of the main challenges in Physics during these four decades. The beautiful results obtained in the past few years by the LHC experiments are a fantastic summary of the Physics observations predicted by the Standard Model.

However, there are several areas where the standard Model has problems, e.g. its lack of precise predictions for the particle masses and lifetimes. Theoretical approaches, such as Lattice QCD [12], compute at best the nucleon mass with one per mille accuracy. The description of the nucleon in terms of valence quarks, sea quarks and gluons is far from optimal. My small brain has always difficulties in imagining a brownian motion of the official nucleon components playing a ping-pong exercise in a mollases. The Parton Distribution Functions (PDF) coming from the deep inelastic experiments are complex when used in the analysis of LHC data. Far too many parameters are required to match the experimental results. Even a simple process such as proton-proton elastic scattering requires complex explanations. As an example no theoretical model was able to predict accurately the results from TOTEM [13]. These partons distribution functions were perfect at a time where computing was in the infancy and only a brownian motion proposed. The model with a few quarks was OK when only a few ten of particles was known. It is not appropriate anymore today with several hundred particles discovered.

Nature very often offers very interesting observations such as the mass difference between charged and neutral particles, the fact that the neutron has a small negative charge vanishing only after a few fermis in contrast with the sharp change for the proton or the fact that the neutron is stable when bound in a nucleus. I have always been puzzled by the fact that all particles decay into electrons, photons, neutrinos or the stable proton. Being constituted of other particles means being a bound state of these particles, at the exception of the photon. Quantum field theoretic processes have no problem turning one kind of particles into other kinds of particles. When looking at the Feynman diagram **Figure 1**, I see two conceptual problems: virtuality and Schrodinger cats. Mathematically speaking, it is simple to show the virtual W boson decaying into final products, here electron and neutrino can be dead or alive in the muon or W! This simple observation was a strong incentive to develop the nuon model described in the following chapters.

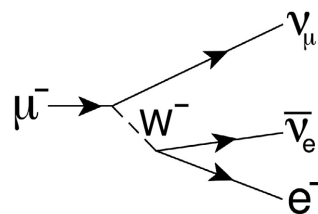


Figure 1. Muon decay diagram.

It is obvious that the proposal for a new model for particle constituents is going to meet very strong objections, to say the least. This work started with a simple idea to evaluate particle masses. Following the initial good results obtained, it was tempting to test the model with well-known physics processes such as elastic scattering. The even better results with this process were a new incentive for more ambitious tests, like the production of particles in proton-proton inelastic collisions at the LHC and jets physics. The next step has been the investigation of the deep inelastic processes and the comparisons with HERA [14] data. One of the last chapters of this paper considers the formation of nuclei and their collisions compared to results in Pb-Pb or Au-Au collisions at CERN or BNL.

The nuons model is not in contradiction with the standard model. It provides an alternative to the quarks/gluons constituents model. Of course, the model must (and it does) reproduce the experimental results traditionally explained by the partons collisions in deep-inelastic scattering and jets physics. The hadron-hadron collisions are interpreted as a convolution of collisions between the leptons of the nuons.

Degrees of freedom, such as introduced later with the nuons, may be understood as elementary ones, related to foundation of the description. But it is not the only possibility. They may be interpreted as an attempt to introduce optimized degrees of freedom, such as a kind used in an interactive picture of a Hamiltonian description. It is generally known, that symmetries and resulting relations may not be of elementary level, but may be the consequence of dynamic, often of stochastic nature. If indeed it is the case one may shed the light on difficult non-perturbative domains. Establishing possible interpretations of the system presented in the later sections is out of scope of this present work. Independently, if the presented results may lead to alternative and/or equivalent picture of Standard Model and its elementary fields, or to better control properties of dynamic processes, it is of importance to collect and present observations in a systematic way. Of course, a valid possibility is that this is just collection of puzzling but otherwise accidental features. This work is organized as follows.

2. The Nuon Model

As illustrated in **Figure 2**, if one considers only the final and stable states, all particles decay into $\nu_e, \bar{\nu}_e, \nu_\mu, \bar{\nu}_\mu, e^+, e^-, \gamma$ or protons. This looks like an incentive to imagine a model where particles are built out of these basic building

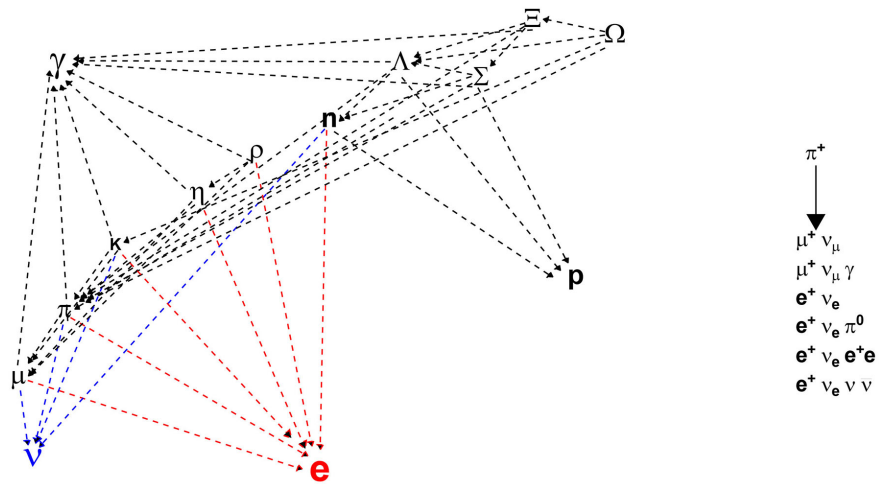


Figure 2. Particles decay examples (left) and π^+ decays (right).

blocks, except the photon that is the result of an intermediate process. When looking more precisely into all possible decay branching modes, it becomes intuitive to imagine an intermediate system, here called a nuon, with which all other particles can be built. We assume a nuon (contraction for neutrinos and electrons) to be a very stable bound state $[e^+ \nu_e \bar{\nu}_e]$ behaving like a neutrino when it is free and not bound itself inside a particle because protected by the neutrinos acting as a possible shielding material. Each nuon inside a particle can be considered as a dipole rotating around the axial nuons of this particle and its positron and electron are subject to electromagnetic interactions with their counterparts in other nuons.

Nature is full of examples where structures are stable for a given scale and temperature, for example atoms, molecules, cells, animals, planets, solar systems, galaxies. Concerning the nucleon, one assumes that around one billionth of a second after the big bang, the temperature/pressure/energy combination was such that the quarks and the gluons were in a regime where they could stabilise. In this model, it is assumed that under these conditions, stable nuons could form structures such as muons, pions, kaons, protons, etc.

Giving this assumption, let's see now how these nuons can assemble into units of N nuons assuming only electromagnetic-type interactions between the dipoles electron/positron of the respective nuons. The units (*i.e.* particles) are assumed to have a spherical shape. In fact it could be any shape, an ellipsoid, but while testing different models, the sphere proved to be the simplest and most intuitive that still gives nice results. For each particle, we assume $N - 2$ nuons rotating around an axis consisting of 2 nuons. In addition the nuons rotate around themselves and their own axis points to the centre of the particle. Just to give a simple example at this point, the proton is built with 64 nuons rotating around the 2 axis nuons and a pion has 4 nuons rotating around the 2 axial nuons. Particles can be seen as solenoids built with N rotating dipoles. In the section on p-p elastic scattering we will see that an estimation of the rotation speed of the non

axial nuons is about 0.06^*c . This rotation speed is also in perfect agreement with the angular velocity when computing the magnetic moment of the proton, neutron or muon. Its low absolute value is also interesting because it does not require complex relativistic corrections. Positive particles are built with $N - 2$ nuons, 2 axial nuons and a positron at the centre of the sphere. The radial nuons have their electrons near the centre and their positron near the outside radius, a neutrino is very close to the centre and an antineutrino between the electron and the positron. The axial line of a positive particle has a one central positron, 2 electrons, 2 positrons + N neutrinos. Negative particles have an electron at the centre and an opposite configuration for the radial nuons. During the original design, it was expected that the neutral particles will have nothing at their centre, but this case proved not to work. The minimisation system could not find any convergent point. Instead the only possible configuration found was to place a system $e^+ \overline{\nu}_e e^-$ or $e^+ \nu_e e^-$ (eg for a neutron and antineutron respectively). This configuration provides too an easy explanation for the neutron decay $n \rightarrow p + \overline{\nu}_e + e^-$. In this model, the electron, positron and neutrino components of the nuon are like the *partons* of the classical model.

2.1. Goals and Constraints

A new model for particles needs to be coherent with proven observables:

- It must be able to predict as accurately as possible particles mass, radius, magnetic moment (if any), binding energy, life time.
- It must be able to predict or be consistent with the results of various collision/interaction types, e.g. elastic scattering, hard collisions with precise generation of the collision products, particle types, kinematics and jets.
- It must be able to test the particles components geometry and density with results e.g. of the deep inelastic experiments.
- It must be predictive when tested at new collision energies or configurations.
- The number of parameters in the model must be as small as possible.

2.2. Making Particles

Assuming N nuons in a cube with a side of about 1 fermi, we generate nuons at random positions inside the cube, then using the MINUIT [15] system part of the ROOT library we minimise the function $F = F_C + \alpha F_G$ where F_C is the sum of the Coulomb forces at the centre of the particle and F_G is the deviation from a spherical shape and α is a normalisation factor. Each nuon is at position (x_i, y_i, z_i) with radius $r_i = \sqrt{x_i^2 + y_i^2}$ and $R_i = \sqrt{x_i^2 + y_i^2 + z_i^2}$. z is by definition the axis joining the 2 axial nuons (see **Figure 3**). $F_C = \sum q_i q_j / r_{ij}^2$ and $F_G = \sum (r_{mean}^2 - r_i^2)$ where r_{mean} is a free parameter representing the sphere radius. So, the input to MINUIT is a system with $3*N + 2$ free parameters and the 2 conditions of F (3 parameters for each nuon, the $3N + 1$ th parameter is the sphere radius and the $3N + 2$ is the distance between the electron and the positron expressed in percentage of the radius). In fact, the condition that F_C

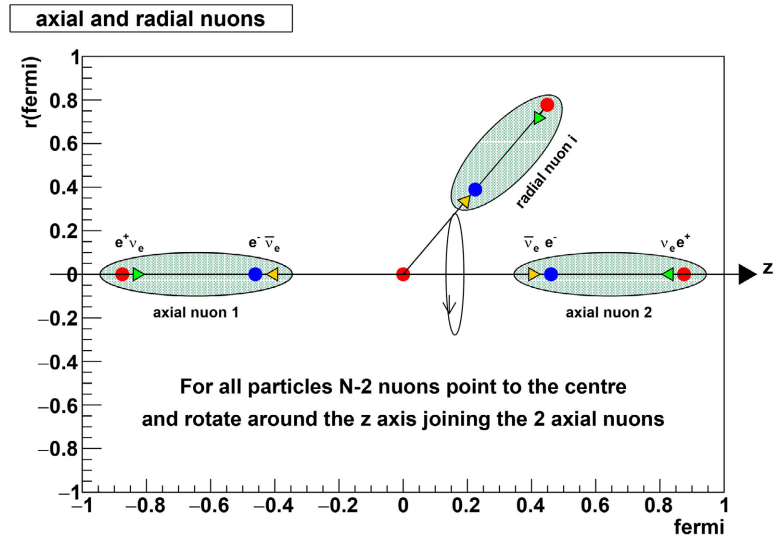


Figure 3. Axial and radial nuons schema.

must be minimal at the centre of the particle is only one among many other possibilities that have been tested. What we see in reality with the 2 conditions F_C and F_G is that the problem is somehow equivalent to finding a sphere where N objects are equidistant on its surface. Instead of this materialist point to point approach a more elegant probabilistic but difficult approach using quantum mechanics could have been developed.

A program *findall* has been initially written to compute all cases for $5 < N < 150$, then expended to compute the masses of all known mesons and baryons for $5 < N < 785$. MINUIT minimizes the function F and finds the best values for the $3N + 2$ parameters. What we observe is quite interesting. At the end of the minimisation process the nuons have moved to stable positions inside the particle, in most cases reproducing configurations with a lot of symmetry (see later), pentagons, hexagons, decagons, and/or combinations of all these basic figures. F has smaller values for particles with the highest symmetries. For a given value of N , several solutions are possible and all values of N give at least one solution.

2.3. Computing Particle Masses

Because the system is built with $N - 2$ nuons rotating around the 2 axial nuons, we compute the inertia of the system $I = \sum m_i r_i^2$ and its total energy (mass) $M = I\Omega^2$ where Ω is the angular speed $\Omega = v/(2\pi R)$. Two parameters are used in this computation: the electron mass and a global normalisation coefficient.

When looking at the results we see that the obtained mass values lie nicely on a straight line (see Figure 4). This not surprising as it is easy to demonstrate that when n points are distributed on the surface of a sphere $\sum (x_i^2 + y_i^2) / R^2 = \frac{2n}{3}$. From this figure we conclude that the best mass match for a proton corresponds to $N = 64 + 2$, i.e. the case where 64 radial nuons rotate around 2 axial nuons.

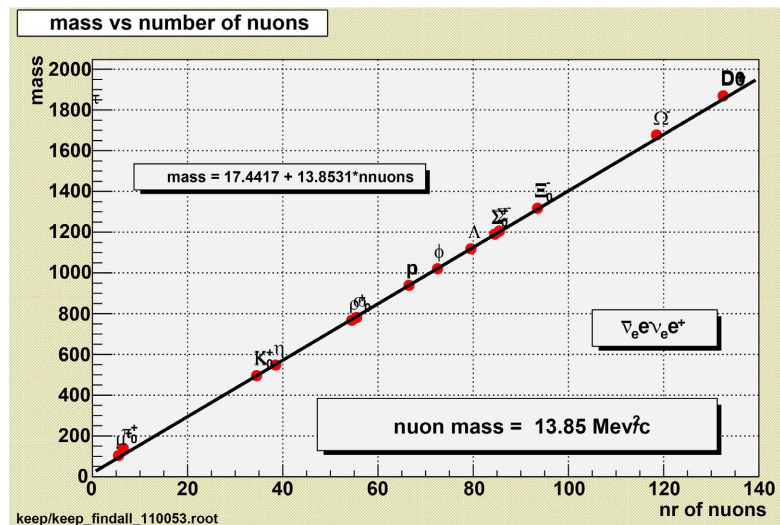


Figure 4. Particles Mass vs number of nuons + 2.

Then we can build the *Mendeleev*-like table shown in Figure 5 for the case of 20 particles ranging from the muon with 3 + 2 nuons, the pion with 4 + 2, the kaon with 32 + 2, up to the D_0 with 130 + 2. As one can see in the column (PDG – nuons)/PDG the relative error on the mass is at the per mile level or better when compared to the PDG tables [16]. Also note the very precise calculation of the neutral vs charged particle mass with the same number of nuons. This behaviour is in particular very striking for (π, π_0) , (K^+, K_0) , (p, n) , (D^+, D_0) . The muon and pion masses are predicted with a relative precision of 10^{-7} .

Using a simple line fit, we can say that the mass of a particle made of N nuons is proportional to N with $mass_N = 18 + 13.84 * N$, *i.e.* that the nuon mass is about $13.84 \text{ MeV}/c^2$. The nuon mass is likely due to a system rotating at high speed around the nuon axis.

The linearity shown later in Figure 4 has been observed in the past by several authors, see for example KOIDE [17] or GREULICH [18] or PAASCH [19]. The particle masses seem to be in a first approximation (with a precision of a few per cent) a function of a running number N . In a following section, we will see that the same program has been used to compute the masses for a much larger number of particles (135 mesons and 133 baryons). The linear fit for these 268 particles gives a very close result, around $14 \text{ MeV}/c^2$ per nuon.

The muon is considered as a composite object and a *neutral* muon μ_0 is emerging with a mass = $101.565 \text{ MeV}/c^2$. It could be that this neutral particle decays with similar channels than the π_0 with the missing energy attributed to a neutrino? An interesting debate!

In Figure 6, a proton is represented with indications of the size and the direction of the force for each external positron. In Figure 7(left) we show a zoom on a front view (radial view) of a proton exhibiting the positrons outside the *nuon-spoke*, the electrons inside and neutrinos, antineutrinos as double cone objects in yellow and blue respectively. On the picture (right) we show a neutron with the same perspective.

| nuons | quarks | spin | rings | PDG mass (MeV/c ²) | nuons model mass (MeV/c ²) | PDG-nuons PDG | mmexp/mm _q (μn) | mm_nuons (μn) | epot_energy (MeV) | life time PDG (seconds) |
|-------------------------------|--|------|-------|--------------------------------|--|--------------------|----------------------------|---------------|-------------------|-------------------------|
| μ ⁺ ₃ | | 1/2 | 1 | 105.658 | 105.658 [6e-06] | 1.780e-07 (4875) | 8.89/?? 0 | 8.892 | 0 ± 0 | 2.2e-06 |
| π ⁺ ₄ | u \bar{d} | 0 | 1 | 139.570 R = 0.657 | 139.570 [5e-06] R = 0.633855 | 9.060e-07 (4873) | ?? 0 | 0.000 | 0 ± 0 | 2.6e-08 |
| π ₀ ₄ | (u \bar{u} -d \bar{d})/√2 | 0 | 1 | 134.977 | 134.977 [0] | 6.258e-07 (4869) | -?? 0 | 0.000 | 0 ± 0 | 8.4e-17 |
| K ⁺ ₃₂ | u \bar{s} | 0 | 2 | 493.677 | 493.586 [0.42] | 1.852e-04 (29191) | ?? 0 | 0.000 | 0 ± 0 | 1.24e-08 |
| K ₀ ₃₂ | d \bar{s} | 0 | 2 | 497.611 | 497.279 [0.53] | 6.667e-04 (30462) | -?? 0 | 0.000 | 0 ± 0 | 5.11e-08 |
| η ₃₆ | (u \bar{u} +d \bar{d} -2s \bar{s})/√6 | 0 | 2 | 547.862 | 547.894 [1.5] | -5.920e-05 (30775) | -?? 0 | 0.000 | 0 ± 0 | 3.5e-08 |
| p ₆₄ | uud | 1/2 | 3 | 938.272 R = 0.8768 | 938.272 [0.73] R = 0.875718 | 1.447e-08 (26941) | 2.793/2.79 0 | 2.790 | 0 ± 0 | 1e+40 |
| n ₆₄ | udd | 1/2 | 3 | 939.565 | 939.536 [0.88] R = 0.831374 | 3.079e-05 (27469) | -1.913/1.86 0 | -1.958 | 0 ± 0 | 885.7 |
| φ ₇₀ | s \bar{s} | 1 | 4 | 1019.461 | 1019.913 [0.3] | -4.431e-04 (4853) | -?? 0 | -1.806 | 0 ± 0 | 1.55e-22 |
| Λ ₇₇ | uds | 1/2 | 4 | 1115.683 | 1117.473 [0.27] | -1.604e-03 (4807) | -0.613/0.61 0 | -1.646 | 0 ± 0 | 2.63e-10 |
| Σ ⁺ ₈₂ | uus | 1/2 | 4 | 1189.370 | 1190.979 [1.2] | -1.353e-03 (1343) | 2.458/2.69 0 | 2.587 | 0 ± 0 | 8.02e-11 |
| Σ ₀ ₈₂ | uds | 1/2 | 4 | 1192.640 | 1188.514 [0.97] | 3.460e-03 (1334) | -0.61/0.82 0 | -1.545 | 0 ± 0 | 7.4e-20 |
| Ξ ⁻ ₉₁ | dss | 1/2 | 4 | 1321.710 | 1318.579 [0.62] | 2.369e-03 (1248) | -0.651/0.51 0 | -2.515 | 0 ± 0 | 1.64e-10 |
| Ξ ₀ ₉₁ | uss | 1/2 | 4 | 1314.860 | 1314.985 [0.73] | -9.521e-05 (1423) | -1.25/1.44 0 | -1.393 | 0 ± 0 | 2.9e-10 |
| Ω ⁻ ₁₁₆ | sss | 3/2 | 5 | 1672.450 | 1671.816 [0.53] | 3.788e-04 (1258) | -2.02/1.83 0 | -2.381 | 0 ± 0 | 8.21e-11 |
| D ⁺ ₁₃₀ | c \bar{d} | 0 | 5 | 1869.660 | 1871.083 [0.48] | -7.613e-04 (1191) | ?? 0 | 0.000 | 0 ± 0 | 1.04e-12 |
| D ₀ ₁₃₀ | c \bar{u} | 0 | 5 | 1864.840 | 1864.080 [0.5] | 4.075e-04 (1351) | -?? 0 | 0.000 | 0 ± 0 | 4.1e-13 |

kDz0 = 0.63026 kMass = 17.2878 kDrpm = 0.0062 kNdrp = 0.28503 kBeta = 0.05968

6.950e-04

Figure 5. Particles mass and magnetic moment.

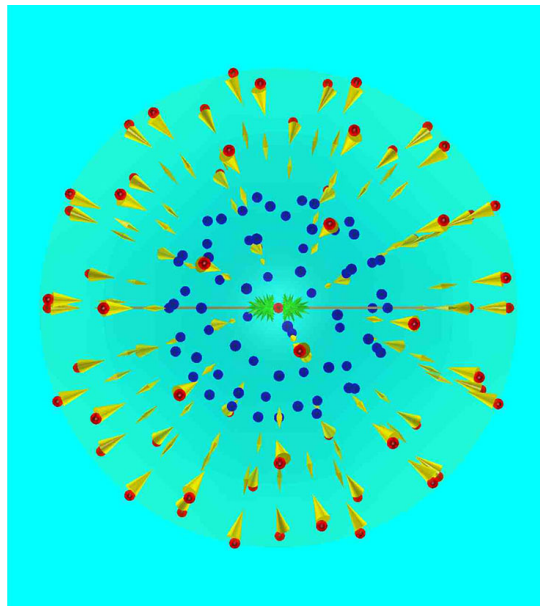


Figure 6. Coulomb forces at the position of the external positrons. The size of the cone is proportional to the force and the cone axis indicates the direction of the force.

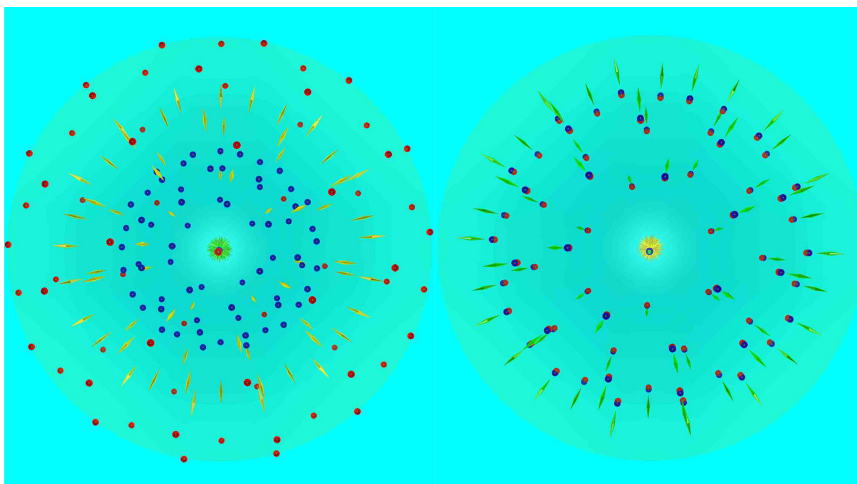


Figure 7. Proton (left) and Neutron (right) front view. Red circles are positrons, dark blue circles are electrons, yellow cones are antineutrinos and green cones are neutrinos.

2.4. Determination of the Proton Radius vs. Proton Energy

There are at least two reasons to select the case $N = 64$ radial nuons + 2 axial nuons for the proton and neutron. It is the only combination that gives a precise mass at rest for the proton (0.938276 GeV) for a radius of 0.876 fermi. As we will see later, the orbital rotation speed has been found to be $0.05968 * c$, the best value explaining the shape of the *dip* for the proton-proton elastic scattering at 7 TeV. This value combined with the proton radius gives also a perfect match for the proton magnetic moment (see later). Since the first experiments at the *ISR* we know that the elastic and inelastic proton-proton cross-sections are rising with the collision energy. For example the elastic cross-section has been measured and parameterized by TOTEM [13] to be

$$f_{ppel} = 11.84 - 1.617 * \ln(s) + 0.1359 * \ln^2(s)$$

where s is the square of the collision energy. In the following chapters we will use this formula to estimate the proton radius as a function of the collision energy. We take $R = k\sqrt{f_{ppel}}$ and we compute the parameter k such that $R = 0.876$ fermi for $\sqrt{s} = 20$ GeV.

2.5. Computing Magnetic Moment

In **Figure 5** two columns with labels “ mm_{exp}/mm_q ” and “ mm_nuons ” are shown with results expressed in nuclear magnetic moments (μ_n). The “ mm_{exp} ” are the experimental values for particles with a magnetic moment. The “ mm_q ” are the values from the quark model. The “ mm_nuons ” values are the results from the nuons model. The magnetic moment is simply $mm = \sum q_i r_i v_i$ where q_i, r_i, v_i are respectively the charge, the orbital radius and speed of the electron or positron of nuon i . A nuon has a positron with charge $q = 1$ at radius rp and velocity vp and an electron $q = -1$ at radius re and velocity ve . We set $vp = kBeta * rp/R$ where $kBeta$ and R are respectively the velocity of the most

external positron or electron of the particle and R its radius. In the same way for the electron, we set $ve = kBeta * re/R$. So the magnetic moment of one orbiting nuon is $mn = kBeta * (rp^2 - re^2)/R$. We find that $kBeta = 0.05968$ gives a perfect value for the muon, proton and neutron magnetic moment. This value is also in agreement with the value used for the proton-proton elastic scattering and also the value of a distance parameter used in inelastic proton-proton interactions as we will see later. The total magnetic moment for a charged particle is the sum of magnetic moments of its nuons plus (the magnetic moment of the central electron or positron)*particlemass/protonmass. For neutral particles we add the magnetic moments of the nuons and the magnetic moment of the bound electron-positron system at the center. This works well for the neutron, but it looks like for other neutral particles we have to assume that the contribution from the central system vanishes.

The top part of **Figure 8** shows the radius of the positive (in black) and neutral particles (in red) as a function of N . The bottom part of the picture shows the density plot of the z positions of the nuons vs N for $5 < N < 120$ with an indication where the standard particles lie. In **Figure 9** we show a few cases μ ($N=5$), π ($N=6$), K ($N=34$), p ($N=66$), Λ ($N=79$), Ξ ($N=93$), Ω ($N=118$) from a data base of a few hundred particles for each value of N . On the left side we display the histogram of the z positions of the centre of the nuons with in green the z position of the 2 axial nuons, in red the z position of the centre of the nuons for neutral particles and in blue for charged particles. We see that the muons have 3 radial nuons orbiting at $z = 0$, the pions 4 orbital nuons also at $z = 0$, the kaons have 2 major z positions on each side of the z axis, the protons have 3, etc. The second column shows the radial views (y vs x), the third column a 3-D scatter-plot view x, y, z for many particles with the given N . Each peak along

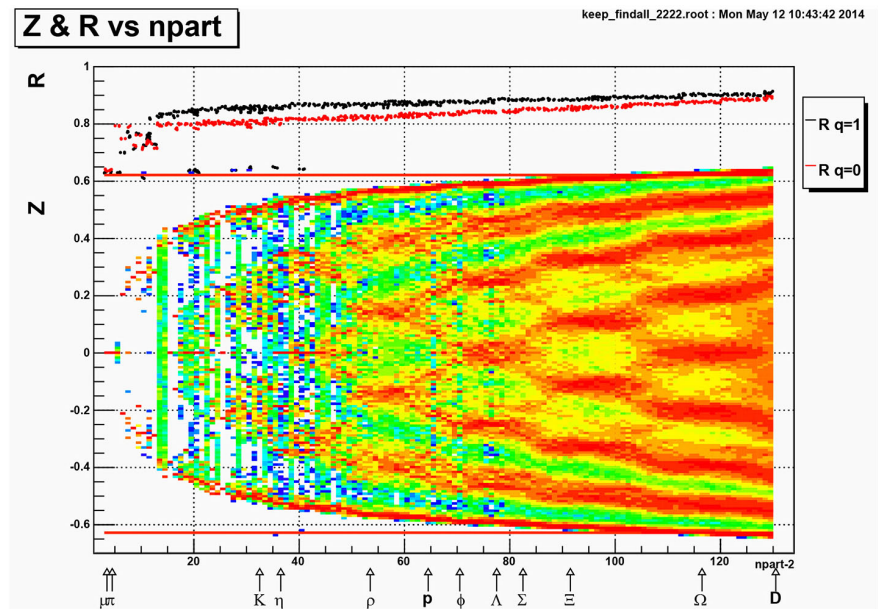


Figure 8. Particle radius vs N (top), z vs N (bottom).

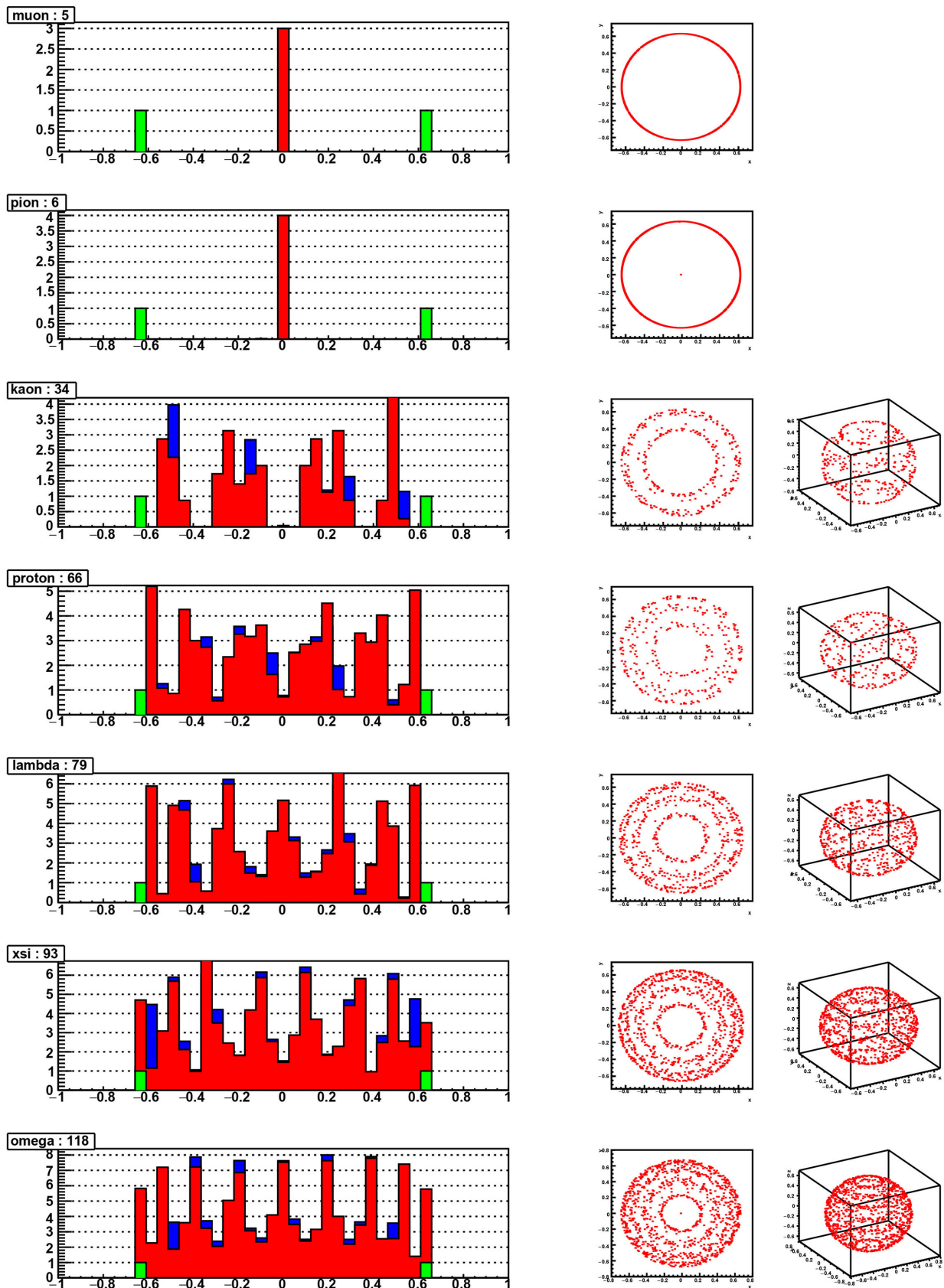


Figure 9. Some particles.

z has a Gaussian distribution and any z value in the same ring generates about the same value for the minimisation function F described above. At this point note that assuming an ellipsoidal shape instead of a spherical shape for N greater than 66 generates more symmetric and stable results. However because the computation time is already pretty high when using a simple sphere model, it is multiplied by a large factor when using an ellipsoid. The computation time becomes proportional to N^3 instead of N^2 . For example the minimization time for a proton ($N = 66$) is about 10 seconds and it took several weeks to compute a data base of particles of a reasonable size for the work described in the following sections. It is indeed possible to improve the computation time in the future and test the expected benefits of an ellipsoid model instead of a sphere with far more statistics for the masses well above the proton mass.

2.6. Particles Stability and Life-Time

In the results shown in **Figure 5** only 20 well known particles are shown. However the program converges for many more values. It is interesting to note that for all values of N from 7 to 33 the F value is bad. This is easy to understand. The muon ($N - 2 = 3$) and pion ($N - 2 = 4$) are systems with only one ring with all x , y nuon positions being at $z = 0$ for the radial nuons. Making 2 rings such as the kaon ($N - 2 = 32$) requires larger values of N . The investigation of the particles stability and life-time requires more work. During the minimisation process with MINUIT, local minima are observed. Understanding these local minima is a prerequisite to continue the work on particles life time.

Figure 10 shows the force vs radius in case of a proton.

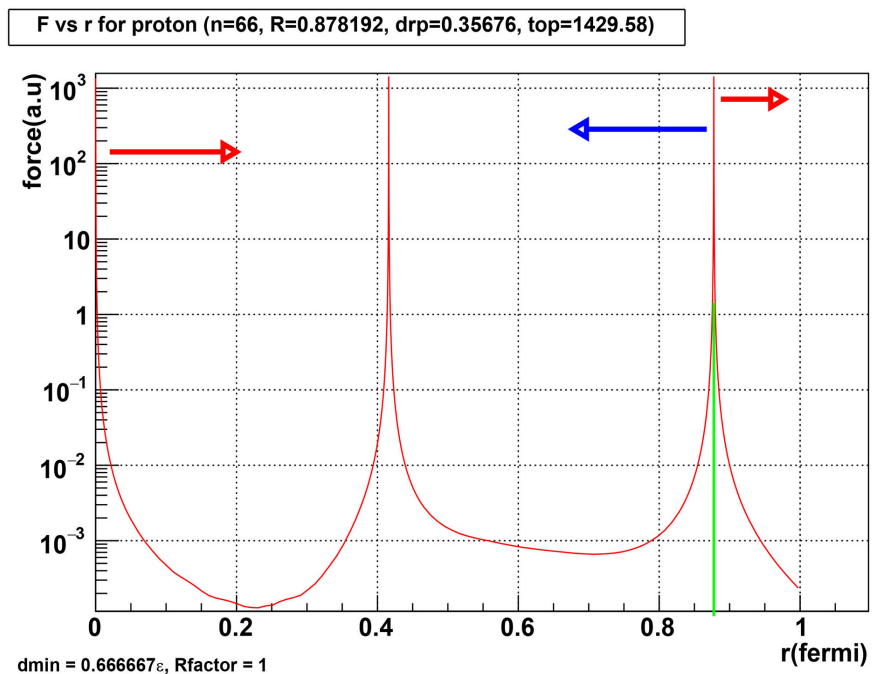


Figure 10. Attractive/repulsive forces in proton vs radius.

2.7. Nuons, Quarks/Gluons and the Strong Force

At a first glance, the nuon model appears to contradict the conventional quark/gluons model. However, as we will see in the section about charge density in the neutrons, quarks are seen in a nucleon from the nuon model perspective as objects having only a statistical behaviour and not a concrete object behaviour. In the same way the gluons properties and the strong force are just macroscopic properties of something described in more detail with the nuons. In particular, we will see in the section on p-p elastic scattering that the nuon model reproduces very precisely the experimental results for p-p and p- \bar{p} elastic scattering for energies ranging from $\sqrt{s} = 27.43 \text{ GeV}$, as seen at the ISR, to $\sqrt{s} = 13 \text{ TeV}$, at the LHC/TOTEM.

When colliding protons against protons (see later), we see the interactions of the electrons/positrons inside the nuons of the respective protons. In a sense a proton is just a highly symmetric and beautiful assembly of electron/positron pairs (dipoles). In the current collisions model, neutrinos and antineutrinos are ignored, at the exception of the neutrinos on the rotation axis. Colliding protons is a bit like colliding quarks and gluons in p-p collisions or one or more electron/positron pair in an e^+e^- collider with 3 possible cases:

- Radial electron/positron of first proton against radial electron/positron of second proton.
- Radial electron/positron of first proton against the 2 axial nuons of the second proton, *i.e.* 2 electrons + 3 positrons + 66 neutrinos. Similar to the first case, but the collision involves more energy.
- 2 axial nuons of first proton against 2 axial nuons of second proton. This special case carries of course a lot more energy as it is the equivalent of $2(5e^+e^- + 66 \text{ neutrinos})$ collisions.

Jets appear as soon as the electrons get very close. To calculate at this point the amount of energy involved, one can make a very rough estimate that, for example at $\sqrt{s} = 7 \text{ TeV}$ each nuon is about $7000/(2 * 66) = 53 \text{ GeV}$ if one assumes that the energy is distributed evenly across all nuons. When analyzing the dynamics of the proton-proton collisions, we see that the total energy of all radial nuons is about 73 per cent of the total energy and the remaining 27 percent is carried by the axial nuons. More precisely the fraction of the proton-proton energy in central collisions is

$$k_{Axial} = (66 + 6 + 1)/(66 * 4 + 1) = 0.275472 .$$

This gives a maximum energy $\text{maxPt} = k_{Axial}\sqrt{s}$ for the axial-axial collisions of 540 GeV for a pp collider at 1.96 TeV, 1.93 TeV for a pp collider at 7 GeV and 3.58 TeV for a pp collider at 13 GeV, see **Figure 11**. Based on this simple construction parameter, a maximum Pt for jets is, by definition, equal to maxPt , and this prediction is confirmed by all experimental results, in particular by the latest results at the LHC over more than 10 orders of magnitude, as we will see later.

The electrons/positrons (Figure 12) are assumed to behave like a gaussian wave with a standard deviation $kElecSigma = \epsilon$ equal to about 0.0001 fermi.

Figure 13 illustrates how the elastic, deep and highly inelastic cases are taken into account during the simulations. Highly inelastic collisions are generated when two waves are very close (distance $d < kElecSigma$). Elastic interactions require $d > 30 kElecSigma$. Of course, all possible cases may be encountered, e.g. in a proton-proton collision at the LHC energies.

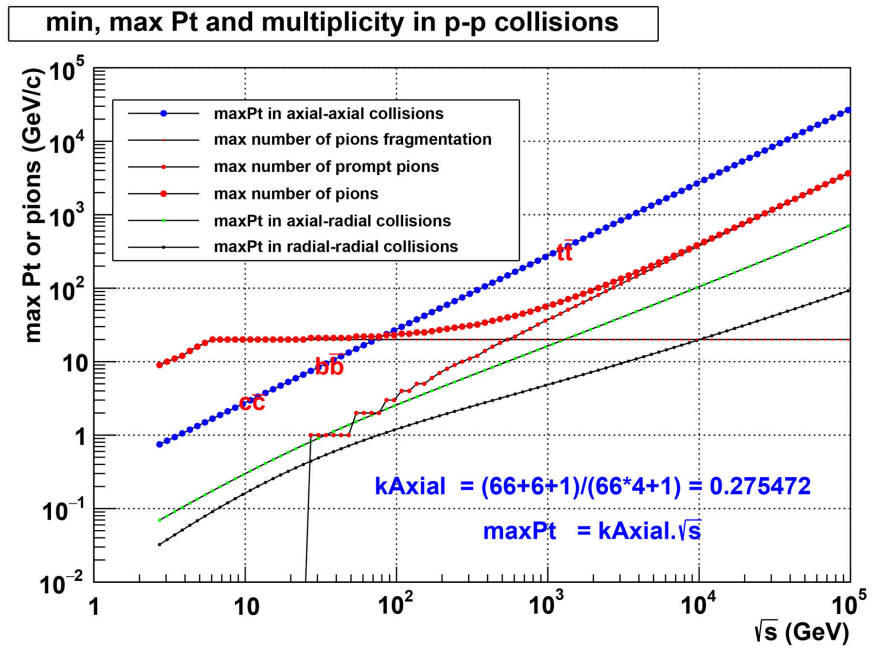


Figure 11. Maximum energy per type of collision and maximum number of pions.

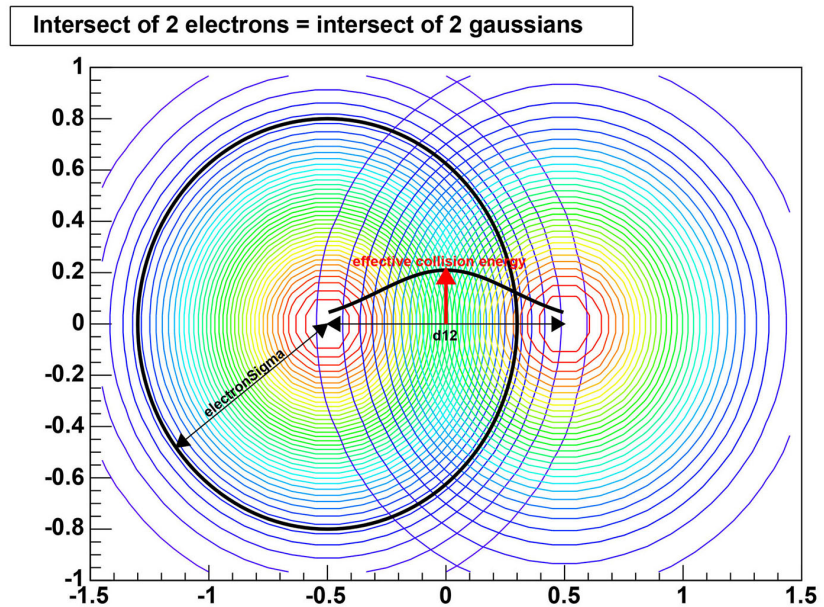


Figure 12. Colliding electrons. Each electron is taken as a gaussian with standard deviation $electronSigma$.

3. Computing Masses of All Know Mesons and Baryons

The Particle Data Group PDG [16] is reporting each year the status of the known mesons and baryons. The PDG tables in the 2022 version include 135 mesons and 133 baryons. The program findall has been extended to compute the masses of all particles reported in this last issue. The following **Figure 14** shows the masses of all mesons and baryons versus the number of nuons per particle. The complete results are shown in **Figure 15** and **Figure 16**.

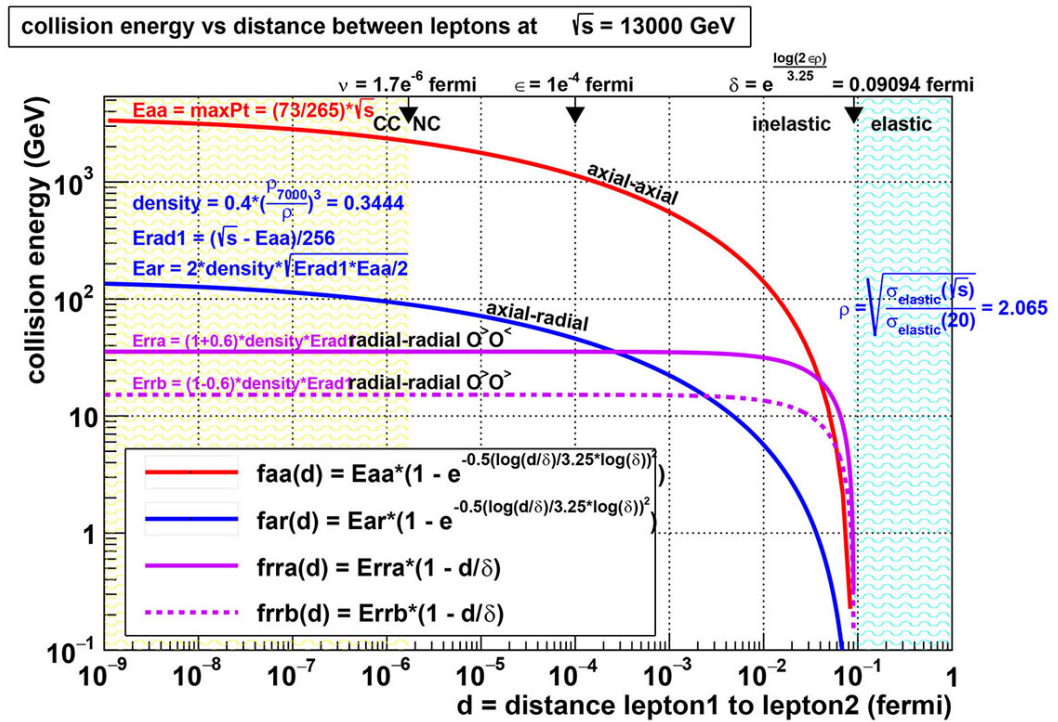


Figure 13. Energy generated by axial-axial, axial-radial or radial-radial electron/positron collisions as a function of the distance between the colliding objects.

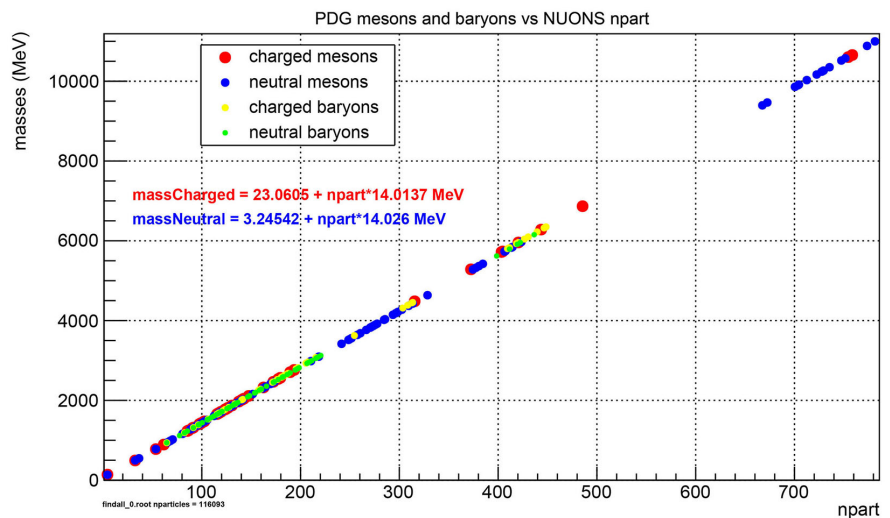


Figure 14. PDG mesons and baryons vs the number of nuons per particle.

| name | PDG mass | N | nuons mass | rerr | name | PDG mass | N | nuons mass | rerr | name | PDG mass | N | nuons mass | rerr |
|------------------------------------|----------|------------------|------------|----------|-----------------------------------|----------|-------------------|------------|----------|----------------------------------|----------|------------------|------------|----------|
| --- Light Unflavored Mesons | | | | | --- Strange Mesons | | | | | --- Bottom Charged Mesons | | | | |
| π^+ | 139.57 | 4 _v | 139.57 | 2.4e-06 | K^+ | 493.68 | 32 _v | 493.65 | 4.5e-05 | B_c^+ | 6274.47 | 443 _v | 6280.20 | -9.1e-04 |
| π_0 | 134.98 | 266 _v | 134.98 | 2.1e-06 | K^0 | 497.61 | 1560 _v | 497.31 | 6.0e-04 | $B_c(2S)^+$ | 6871.20 | 485 _v | 6867.14 | 5.9e-04 |
| η | 547.86 | 36 _v | 547.94 | -1.3e-04 | $K^*(892)$ | 891.66 | 61 _v | 892.52 | -9.6e-04 | --- Ccbar Mesons | | | | |
| $\rho(770)^+$ | 775.26 | 53 _v | 778.93 | -4.7e-03 | $K_1(1270)$ | 1253.00 | 86 _v | 1246.49 | 5.2e-03 | $\eta_c(1S)$ | 2983.90 | 210 _v | 2984.60 | -2.3e-04 |
| $\omega(782)$ | 782.65 | 53 _v | 781.23 | 1.8e-03 | $K_1(1400)$ | 1403.00 | 97 _v | 1403.36 | -2.6e-04 | $J/\psi(1S)$ | 3096.90 | 218 _v | 3096.28 | 2.0e-04 |
| $\eta(958)$ | 957.78 | 65 _v | 950.03 | 8.1e-03 | $K_1(1410)$ | 1414.00 | 98 _v | 1417.60 | -2.5e-03 | $\chi_{c0}(1P)$ | 3414.71 | 241 _v | 3417.56 | -8.3e-04 |
| $f_0(980)$ | 990.00 | 68 _v | 991.01 | -1.0e-03 | $K_2^*(1430)$ | 1425.00 | 99 _v | 1431.83 | -4.8e-03 | $\chi_{c1}(1P)$ | 3510.67 | 248 _v | 3515.71 | -1.4e-03 |
| $a_1(980)$ | 980.00 | 67 _v | 977.63 | 2.4e-03 | $K(1680)$ | 1718.00 | 119 _v | 1714.42 | 2.1e-03 | $h_c(1P)$ | 3525.38 | 249 _v | 3529.81 | -1.3e-03 |
| $\phi(1020)$ | 1019.46 | 70 _v | 1019.91 | -4.4e-04 | $K_2^*(1770)$ | 1773.00 | 123 _v | 1772.01 | 5.6e-04 | $\chi_{c2}(1P)$ | 3556.17 | 251 _v | 3557.68 | -4.2e-04 |
| $h_1(1170)$ | 1166.00 | 80 _v | 1160.82 | 4.4e-03 | $K_3^*(1780)$ | 1779.00 | 124 _v | 1785.91 | -3.9e-03 | $\eta_c(2S)$ | 3637.50 | 257 _v | 3641.37 | -1.1e-03 |
| $b_1(1235)$ | 1229.50 | 85 _v | 1232.64 | -2.6e-03 | $K_2^*(1820)$ | 1819.00 | 126 _v | 1814.24 | 2.6e-03 | $\psi(2S)$ | 3686.10 | 260 _v | 3683.41 | 7.3e-04 |
| $a_1(1260)$ | 1230.00 | 85 _v | 1232.64 | -2.2e-03 | $K_4(2045)$ | 2048.00 | 142 _v | 2041.47 | 3.2e-03 | $\psi(3770)$ | 3773.70 | 266 _v | 3767.05 | 1.8e-03 |
| $f_2(1270)$ | 1275.50 | 88 _v | 1273.01 | 2.0e-03 | --- Charmed Mesons | | | | | $\psi(3823)$ | 3822.20 | 270 _v | 3823.41 | -3.2e-04 |
| $f_1(1285)$ | 1281.90 | 89 _v | 1286.20 | -3.4e-03 | D^+ | 1869.66 | 130 _v | 1871.04 | -7.4e-04 | $\psi(3842)$ | 3842.71 | 271 _v | 3837.53 | 1.3e-03 |
| $\eta(1295)$ | 1294.00 | 90 _v | 1301.05 | -5.4e-03 | D^0 | 1864.84 | 130 _v | 1864.12 | 3.8e-04 | $\chi(3872)$ | 3871.69 | 273 _v | 3865.07 | 1.7e-03 |
| $\pi(1300)$ | 1300.00 | 90 _v | 1304.57 | -3.5e-03 | $D^*(2007)^0$ | 2006.85 | 140 _v | 2004.33 | 1.3e-03 | $Z_c(3900)$ | 3888.40 | 275 _v | 3893.33 | -1.3e-03 |
| $a_2(1320)$ | 1318.20 | 91 _v | 1317.80 | 3.0e-04 | $D^*(2010)^+$ | 2010.26 | 140 _v | 2012.95 | -1.3e-03 | $\chi(3915)$ | 3921.70 | 277 _v | 3921.29 | 1.1e-04 |
| $f_0(1370)$ | 1370.00 | 95 _v | 1372.27 | -1.7e-03 | $D_0^*(2300)$ | 2340.00 | 164 _v | 2340.98 | -4.2e-04 | $\chi_{c0}(3930)$ | 3922.50 | 277 _v | 3921.29 | 3.1e-04 |
| $\pi(1400)$ | 1354.00 | 94 _v | 1360.06 | -4.5e-03 | $D_0^*(2420)$ | 2420.10 | 170 _v | 2425.10 | -2.1e-03 | $\chi(4020)$ | 4024.10 | 284 _v | 4019.37 | 1.2e-03 |
| $\eta(1405)$ | 1408.80 | 98 _v | 1413.85 | -3.6e-03 | $D_0^*(2430)$ | 2412.10 | 169 _v | 2411.05 | 4.3e-04 | $\psi(4040)$ | 4039.00 | 285 _v | 4033.43 | 1.4e-03 |
| $h_1(1415)$ | 1416.00 | 98 _v | 1413.85 | 1.5e-03 | $D_2^*(2460)^0$ | 2461.10 | 173 _v | 2467.34 | -2.5e-03 | $\chi(4140)$ | 4146.80 | 293 _v | 4145.85 | 2.3e-04 |
| $f_1(1420)$ | 1426.30 | 99 _v | 1428.04 | -1.2e-03 | $D_3^*(2750)^+$ | 2763.10 | 193 _v | 2763.59 | -1.8e-04 | $\psi(4160)$ | 4191.00 | 296 _v | 4187.92 | 7.4e-04 |
| $a_0(1450)$ | 1474.00 | 102 _v | 1473.88 | 8.4e-05 | --- Charmed Strange Mesons | | | | | $\psi(4230)$ | 4220.00 | 298 _v | 4216.15 | 9.1e-04 |
| $\rho(1450)$ | 1465.00 | 102 _v | 1470.88 | -4.0e-03 | D_s^+ | 1968.35 | 137 _v | 1970.71 | -1.2e-03 | $\chi_{c1}(4274)$ | 4274.00 | 302 _v | 4271.63 | 5.5e-04 |
| $\eta(1475)$ | 1475.00 | 102 _v | 1470.88 | 2.8e-03 | D_s^* | 2112.20 | 147 _v | 2112.25 | -2.4e-05 | $\psi(4360)$ | 4368.00 | 309 _v | 4370.24 | -5.1e-04 |
| $f_0(1500)$ | 1506.00 | 105 _v | 1512.17 | -4.1e-03 | D_{s1}^+ | 2317.80 | 162 _v | 2324.24 | -2.8e-03 | $\psi(4415)$ | 4421.00 | 313 _v | 4425.92 | -1.1e-03 |
| $f_2(1525)$ | 1517.40 | 105 _v | 1512.17 | 3.4e-03 | $D_{s0}^*(2317)^+$ | 2317.80 | 162 _v | 2324.24 | -2.8e-03 | $Z_c(4430)^+$ | 4478.00 | 315 _v | 4484.18 | -1.4e-03 |
| $\pi_1(1600)$ | 1661.00 | 115 _v | 1657.33 | 2.2e-03 | $D_{s1}^*(2460)^+$ | 2459.50 | 172 _v | 2466.34 | -2.8e-03 | $\psi(4660)$ | 4630.00 | 328 _v | 4636.30 | -1.4e-03 |
| $a_1(1640)$ | 1655.00 | 115 _v | 1657.33 | -1.4e-03 | $D_{s1}^*(2536)^+$ | 2535.10 | 177 _v | 2537.52 | -9.6e-04 | --- BBbar Mesons | | | | |
| $\eta_2(1645)$ | 1617.00 | 112 _v | 1610.33 | 4.1e-03 | $D_{s2}^*(2573)^+$ | 2569.10 | 179 _v | 2565.78 | 1.3e-03 | $\eta_b(1S)$ | 9398.70 | 667 _v | 9395.31 | 3.6e-04 |
| $\omega(1650)$ | 1670.00 | 116 _v | 1666.36 | 2.2e-03 | $D_{s1}^*(2700)^+$ | 2708.30 | 189 _v | 2706.94 | 5.0e-04 | $\Upsilon(1S)$ | 9460.30 | 672 _v | 9465.85 | -5.9e-04 |
| $\omega_3(1670)$ | 1667.00 | 116 _v | 1666.36 | 3.8e-04 | --- Bottom Mesons | | | | | $\chi_{c0}(1P)$ | 9859.44 | 700 _v | 9859.49 | -5.0e-06 |
| $\pi_2(1670)$ | 1670.60 | 116 _v | 1671.85 | -7.5e-04 | B^+ | 5279.34 | 372 _v | 5284.74 | -1.0e-03 | $\chi_{c1}(1P)$ | 9892.78 | 703 _v | 9898.28 | -5.6e-04 |
| $\phi(1680)$ | 1680.00 | 117 _v | 1680.22 | -1.3e-04 | B^0 | 5279.65 | 374 _v | 5281.64 | -3.8e-04 | $h_b(1P)$ | 9899.30 | 703 _v | 9898.28 | 1.0e-04 |
| $\rho_3(1690)$ | 1688.80 | 117 _v | 1686.00 | 1.7e-03 | B^* | 5324.70 | 377 _v | 5323.79 | 1.7e-04 | $\chi_{c2}(1P)$ | 9912.21 | 704 _v | 9914.51 | -2.3e-04 |
| $\rho(1700)$ | 1720.00 | 120 _v | 1723.10 | -1.8e-03 | $B_1(5721)^+$ | 5725.90 | 403 _v | 5719.54 | 1.1e-03 | $\Upsilon(2S)$ | 10023.26 | 712 _v | 10027.81 | -4.5e-04 |
| $f_0(1710)$ | 1704.00 | 119 _v | 1708.85 | -2.8e-03 | $B_1(5721)^0$ | 5726.10 | 406 _v | 5731.16 | -8.8e-04 | $\Upsilon(1D)$ | 10163.70 | 722 _v | 10167.44 | -3.7e-04 |
| $\pi(1800)$ | 1810.00 | 126 _v | 1814.24 | -2.3e-03 | $B_2^*(5747)^+$ | 5737.20 | 404 _v | 5732.96 | 7.4e-04 | $\chi_{c0}(2P)$ | 10232.50 | 727 _v | 10238.70 | -6.1e-04 |
| $\phi_3(1850)$ | 1854.00 | 129 _v | 1849.40 | 2.5e-03 | $B_2^*(5747)^0$ | 5739.50 | 407 _v | 5745.56 | -1.1e-03 | $\chi_{c1}(2P)$ | 10255.46 | 728 _v | 10252.26 | 3.1e-04 |
| $\eta_2(1870)$ | 1842.00 | 128 _v | 1835.51 | 3.5e-03 | $B_3^*(5970)^+$ | 5964.00 | 420 _v | 5957.69 | 1.1e-03 | $\chi_{c2}(2P)$ | 10268.65 | 729 _v | 10265.92 | 2.7e-04 |
| $\pi_2(1880)$ | 1874.00 | 131 _v | 1877.62 | -1.9e-03 | $B_3^*(5970)^0$ | 5971.00 | 423 _v | 5969.54 | 2.4e-04 | $\Upsilon(3S)$ | 10355.20 | 735 _v | 10351.11 | 3.9e-04 |
| $f_2(1950)$ | 1936.00 | 135 _v | 1933.98 | 1.0e-03 | --- Bottom Strange Mesons | | | | | $\chi_{c1}(3P)$ | 10513.40 | 747 _v | 10518.72 | -5.1e-04 |
| $f_2(2010)$ | 2011.00 | 140 _v | 2004.33 | 3.3e-03 | B_0^s | 5366.88 | 380 _v | 5366.04 | 1.6e-04 | $\chi_{c2}(3P)$ | 10524.00 | 747 _v | 10518.72 | 5.0e-04 |
| $a_4(2040)$ | 1995.00 | 139 _v | 1990.36 | 2.3e-03 | B_1^s | 5415.40 | 384 _v | 5422.09 | -1.2e-03 | $\Upsilon(4S)$ | 10579.40 | 751 _v | 10575.24 | 3.9e-04 |
| $f_4(2050)$ | 2018.00 | 141 _v | 2018.77 | -3.8e-04 | $B_{s1}(5830)^0$ | 5828.70 | 413 _v | 5829.38 | -1.2e-04 | $Z_b(10610)^+$ | 10607.20 | 754 _v | 10604.59 | 2.5e-04 |
| $\phi(2170)$ | 2159.00 | 151 _v | 2158.84 | 7.2e-05 | $B_{s2}(5840)^0$ | 5839.86 | 414 _v | 5843.44 | -6.1e-04 | $Z_b(10650)^+$ | 10652.20 | 758 _v | 10656.82 | -4.3e-04 |
| $f_2(2300)$ | 2297.00 | 161 _v | 2298.83 | -7.9e-04 | | | | | | $\Upsilon(10860)$ | 10885.20 | 773 _v | 10885.34 | -1.3e-05 |
| $f_2(2340)$ | 2345.00 | 164 _v | 2340.98 | 1.7e-03 | | | | | | $\Upsilon(11020)$ | 11000.00 | 781 _v | 10997.90 | 1.9e-04 |

found ok if diff=|massPDG - massNuons| < 8 MeV, very good if diff < 5 MeV, veryvery good if diff < 1 MeV relerrm = 1.42e-03
 findall_0.root nparticles = 116093 ==> nmesonsPDG = 135, nmfoundok = 135, nmverygood = 106, nmveryverygood = 67

Figure 15. PDG mesons masses compared to nuons.

Important Remark 1. One must be very careful with the affirmation that masses show a linear behaviour in function of a given integer. For example, when fitting the 268 particles (masses from 100 MeV/c² to 11,000 MeV/c²) with a number of nuons going from 32 to 782, the distance between adjacent masses will be in average around 14.3 MeV/c². The precision to compute the masses must be better than 14.3/2 MeV/c². See the bottom of the mesons and baryons tables where it is shown that 50 per cent of the masses are calculated with a precision better than 1 MeV/c².

| name | PDG mass | N | nuons mass | rerr | name | PDG mass | N | nuons mass | rerr | name | PDG mass | N | nuons mass | rerr |
|----------------------|----------|---------------------|------------|----------|--|----------|-------------------|------------|----------|---|----------|-------------------|------------|----------|
| --- N Baryons | | | | | --- Σ Baryons | | | | | --- Charmed Baryons | | | | |
| p | 938.27 | 64 ¹³⁴⁴⁷ | 938.29 | -2.2e-05 | Σ ⁺ | 1189.37 | 82 ⁸⁸² | 1190.45 | -9.1e-04 | Λ _c ⁺ | 2286.46 | 159 ¹⁵ | 2281.76 | 2.1e-03 |
| n | 939.57 | 64 ¹³⁶⁹⁶ | 939.50 | 6.5e-05 | Σ ⁻ | 1197.45 | 82 ⁸⁸² | 1190.45 | 5.8e-03 | Λ _c (2595) ⁺ | 2592.25 | 181 ¹⁸ | 2594.03 | -6.9e-04 |
| N(1440) | 1440.00 | 100 ¹⁰ | 1442.55 | -1.8e-03 | Σ ⁰ | 1192.64 | 82 ⁸⁸² | 1188.48 | 3.5e-03 | Λ _c (2625) ⁺ | 2628.11 | 183 ¹⁸ | 2621.86 | 2.4e-03 |
| N(1520) | 1515.00 | 105 ¹⁰ | 1512.17 | 1.9e-03 | Σ(1385)3/2 ⁺ | 1382.80 | 96 ⁹⁶ | 1389.86 | -5.1e-03 | Λ _c (2860) ⁺ | 2656.10 | 185 ¹⁸ | 2650.14 | 2.2e-03 |
| N(1535) | 1530.00 | 106 ¹⁰ | 1526.76 | 2.1e-03 | Σ(1385)3/2 ⁰ | 1383.70 | 96 ⁹⁶ | 1385.96 | -1.6e-03 | Λ _c (2880) ⁺ | 2681.63 | 187 ¹⁸ | 2678.47 | 1.2e-03 |
| N(1650) | 1650.00 | 115 ¹¹ | 1652.49 | -1.5e-03 | Σ(1660)1/2 ⁺ | 1660.00 | 115 ¹¹ | 1657.33 | 1.6e-03 | Λ _c (2940) ⁺ | 2939.60 | 205 ²⁰ | 2933.60 | 2.0e-03 |
| N(1675) | 1675.00 | 117 ¹¹ | 1680.22 | -3.1e-03 | Σ(1670)3/2 ⁺ | 1675.00 | 116 ¹¹ | 1671.85 | 1.9e-03 | Σ _c (2455) ⁰ | 2452.90 | 171 ¹⁷ | 2451.95 | 3.9e-04 |
| N(1680) | 1685.00 | 117 ¹¹ | 1680.22 | 2.8e-03 | Σ(1750)1/2 ⁺ | 1750.00 | 121 ¹² | 1743.17 | 3.9e-03 | Σ _c (2455) ⁺ | 2453.75 | 172 ¹⁷ | 2453.26 | 2.0e-04 |
| N(1700) | 1720.00 | 120 ¹² | 1723.10 | -1.8e-03 | Σ(1775)5/2 ⁺ | 1775.00 | 123 ¹² | 1772.01 | 1.7e-03 | Σ _c (2520) ⁰ | 2517.50 | 176 ¹⁷ | 2523.30 | -2.3e-03 |
| N(1710) | 1710.00 | 119 ¹¹ | 1708.85 | 6.8e-04 | Σ(1910)5/2 ⁺ | 1910.00 | 133 ¹³ | 1913.32 | -1.7e-03 | Σ _c (2520) ⁺ | 2518.41 | 177 ¹⁷ | 2523.27 | -1.9e-03 |
| N(1720) | 1720.00 | 120 ¹² | 1723.10 | -1.8e-03 | Σ(1915)5/2 ⁺ | 1915.00 | 133 ¹³ | 1913.32 | 8.8e-04 | Σ _c (2800) ⁰ | 2792.00 | 195 ¹⁹ | 2792.62 | -2.2e-04 |
| N(1875) | 1875.00 | 131 ¹³ | 1877.62 | -1.4e-03 | Σ(2030)7/2 ⁺ | 2030.00 | 141 ¹⁴ | 2027.19 | 1.4e-03 | Σ _c (2800) ⁺ | 2806.00 | 197 ¹⁹ | 2803.18 | 1.0e-03 |
| N(1880) | 1880.00 | 131 ¹³ | 1877.62 | 1.3e-03 | Σ(2250)7/2 ⁺ | 2250.00 | 157 ¹⁵ | 2253.32 | -1.5e-03 | Σ _c ⁺ (2800) | 2467.94 | 172 ¹⁷ | 2466.34 | 6.5e-04 |
| N(1895) | 1895.00 | 132 ¹³ | 1891.46 | 1.9e-03 | --- Ξ Baryons | | | | | Σ _c ⁰ (2800) | 2470.90 | 173 ¹⁷ | 2467.34 | 1.4e-03 |
| N(1900) | 1920.00 | 134 ¹³ | 1919.77 | 1.2e-04 | Ξ ⁰ | 1314.86 | 91 ⁹¹ | 1314.99 | -1.0e-04 | Ξ _c ⁺ (2800) | 2578.40 | 180 ¹⁸ | 2579.70 | -5.1e-04 |
| N(2060) | 2100.00 | 147 ¹⁴ | 2102.68 | -1.3e-03 | Ξ ⁻ | 1321.71 | 91 ⁹¹ | 1317.80 | 3.0e-03 | Ξ _c ⁰ (2645) ⁺ | 2579.20 | 181 ¹⁸ | 2578.90 | 1.2e-04 |
| N(2100) | 2100.00 | 147 ¹⁴ | 2102.68 | -1.3e-03 | Ξ(1530)3/2 ⁰ | 1531.80 | 106 ¹⁰ | 1526.76 | 3.3e-03 | Ξ _c (2645) ⁰ | 2645.56 | 185 ¹⁸ | 2650.14 | -1.7e-03 |
| N(2120) | 2120.00 | 148 ¹⁴ | 2117.24 | 1.3e-03 | Ξ(1530)3/2 ⁺ | 1535.00 | 106 ¹⁰ | 1530.33 | 3.0e-03 | Ξ _c (2645) ⁺ | 2646.38 | 186 ¹⁸ | 2649.05 | -1.0e-03 |
| N(2190) | 2180.00 | 153 ¹⁵ | 2186.02 | -2.8e-03 | Ξ(1690) | 1690.00 | 117 ¹¹ | 1686.00 | 2.4e-03 | Ξ _c (2790) ⁰ | 2792.40 | 195 ¹⁹ | 2792.62 | -7.8e-05 |
| N(2220) ⁺ | 2250.00 | 158 ¹⁵ | 2256.42 | -2.9e-03 | Ξ(1820)3/2 ⁺ | 1823.00 | 127 ¹² | 1828.61 | -3.1e-03 | Ξ _c (2790) ⁺ | 2794.10 | 196 ¹⁹ | 2789.07 | 1.8e-03 |
| N(2250) ⁻ | 2280.00 | 160 ¹⁶ | 2284.39 | -1.9e-03 | Ξ(1950) | 1950.00 | 136 ¹³ | 1948.01 | 1.0e-03 | Ξ _c (2815) ⁺ | 2816.74 | 197 ¹⁹ | 2820.32 | -1.3e-03 |
| N(2600) | 2600.00 | 182 ¹⁸ | 2593.00 | 2.7e-03 | Ξ(2030) | 2025.00 | 141 ¹⁴ | 2027.19 | -1.1e-03 | Ξ _c (2815) ⁰ | 2820.25 | 198 ¹⁹ | 2816.91 | 1.2e-03 |
| --- Δ Baryons | | | | | --- Ω Baryons | | | | | Ξ _c (2970) ⁰ | | | | |
| Δ(1232) | 1232.00 | 85 ⁸ | 1230.51 | 1.2e-03 | Ω ⁻ | 1672.45 | 146 ¹⁴ | 1671.85 | 3.6e-04 | Ξ _c (2970) ⁺ | 2970.90 | 209 ²⁰ | 2970.48 | 1.4e-04 |
| Δ(1600) | 1570.00 | 109 ¹⁰ | 1568.00 | 1.3e-03 | Ω(2012) ⁻ | 2012.40 | 140 ¹⁴ | 2012.95 | -2.7e-04 | Ξ _c (3055) | 3055.90 | 215 ²¹ | 3054.30 | 5.2e-04 |
| Δ(1620) | 1610.00 | 112 ¹¹ | 1610.33 | -2.0e-04 | Ω(2250) ⁻ | 2252.00 | 157 ¹⁵ | 2253.32 | -5.9e-04 | Ξ _c (3080) ⁺ | 3077.20 | 215 ²¹ | 3074.91 | 7.4e-04 |
| Δ(1700) | 1710.00 | 119 ¹¹ | 1708.85 | 6.8e-04 | --- Exotic Baryons | | | | | Ξ _c (3080) ⁰ | 3079.90 | 217 ²¹ | 3082.45 | -8.3e-04 |
| Δ(1900) | 1860.00 | 130 ¹³ | 1864.12 | -2.2e-03 | #P _c (4312) ⁺ | 4311.90 | 303 ³⁰ | 4315.30 | -7.9e-04 | Ω _c ⁰ | 2695.20 | 189 ¹⁸ | 2691.01 | 1.6e-03 |
| Δ(1905) | 1880.00 | 131 ¹³ | 1877.62 | 1.3e-03 | #P _c (4380) ⁺ | 4380.00 | 308 ³⁰ | 4385.32 | -1.2e-03 | Ω _c (2770) ⁰ | 2765.90 | 194 ¹⁹ | 2760.77 | 1.9e-03 |
| Δ(1910) | 1900.00 | 133 ¹³ | 1905.83 | -3.1e-03 | #P _c (4440) ⁺ | 4440.00 | 312 ³¹ | 4441.77 | -4.0e-04 | Ω _c (3000) ⁰ | 3000.41 | 211 ²¹ | 2998.38 | 6.8e-04 |
| Δ(1920) | 1920.00 | 134 ¹³ | 1919.77 | 1.2e-04 | #P _c (4457) ⁺ | 4457.30 | 313 ³¹ | 4455.53 | 4.0e-04 | Ω _c (3050) ⁰ | 3050.20 | 215 ²¹ | 3054.30 | -1.3e-03 |
| Δ(1930) | 1950.00 | 136 ¹³ | 1948.01 | 1.0e-03 | --- New LHCb baryons | | | | | Ω _c (3065) ⁰ | 3065.46 | 216 ²¹ | 3068.43 | -9.7e-04 |
| Δ(1950) | 1930.00 | 135 ¹³ | 1933.98 | -2.1e-03 | Ω _b (6316) ⁻ | 6315.64 | 446 ⁴⁴ | 6321.99 | -1.0e-03 | Ω _c (3090) ⁰ | 3090.00 | 218 ²¹ | 3096.28 | -2.0e-03 |
| Δ(2200) | 2200.00 | 154 ¹⁵ | 2200.13 | -6.1e-05 | Ω _b (6330) ⁻ | 6330.30 | 447 ⁴⁴ | 6336.06 | -9.1e-04 | Ω _c (3120) ⁰ | 3119.10 | 220 ²² | 3124.53 | -1.7e-03 |
| Δ(2420) | 2450.00 | 172 ¹⁷ | 2453.26 | -1.3e-03 | Ω _b (6340) ⁻ | 6339.71 | 447 ⁴⁴ | 6336.06 | 5.8e-04 | --- Bottom Baryons | | | | |
| --- Λ Baryons | | | | | Ω _b (6350) ⁻ | 6349.88 | 448 ⁴⁴ | 6349.81 | 1.1e-05 | Λ _b ⁰ | 5619.51 | 398 ³⁹ | 5619.47 | 7.1e-06 |
| Λ(1232) | 1115.68 | 77 ⁷ | 1117.46 | -1.6e-03 | Σ _c (2923) ⁰ | 2923.04 | 206 ²⁰ | 2928.69 | -1.9e-03 | Λ _b ⁺ (5912) | 5912.20 | 419 ⁴¹ | 5913.24 | -1.8e-04 |
| Λ(1405) | 1405.10 | 97 ⁹ | 1399.70 | 3.8e-03 | Σ _c (2939) ⁰ | 2938.55 | 207 ²⁰ | 2943.17 | -1.6e-03 | Λ _b ⁰ (5920) | 5919.92 | 419 ⁴¹ | 5913.24 | 1.1e-03 |
| Λ(1520) | 1519.00 | 105 ¹⁰ | 1512.17 | 4.5e-03 | Σ _c (2965) ⁰ | 2964.88 | 209 ²⁰ | 2970.48 | -1.9e-03 | Λ _b ⁺ (6146) | 6146.20 | 436 ⁴³ | 6152.26 | -9.9e-04 |
| Λ(1600) | 1600.00 | 111 ¹¹ | 1595.64 | 2.7e-03 | Xi_cc (Doubly charmed) | | | | | Λ _b ⁰ (6152) | 6152.50 | 436 ⁴³ | 6152.26 | 4.0e-05 |
| Λ(1670) | 1674.00 | 117 ¹¹ | 1680.22 | -3.7e-03 | Ξ _{cc} ⁺⁺ | 3621.20 | 254 ²⁵ | 3625.04 | -1.1e-03 | Σ _b ⁺ | 5810.56 | 410 ⁴¹ | 5816.79 | -1.1e-03 |
| Λ(1690) | 1690.00 | 118 ¹¹ | 1694.63 | -2.7e-03 | --- Bottom Baryons | | | | | Σ _b ⁰ | 5830.32 | 411 ⁴¹ | 5827.98 | 4.0e-04 |
| Λ(1800) | 1800.00 | 125 ¹² | 1793.38 | 3.7e-03 | Λ _b ⁺ (6097) | 6095.80 | 430 ⁴³ | 6095.00 | -3.6e-04 | Σ _b ⁻ | 5797.00 | 409 ⁴⁰ | 5803.38 | -1.1e-03 |
| Λ(1810) | 1790.00 | 125 ¹² | 1793.38 | -1.9e-03 | Λ _b ⁰ (5935) ⁻ | 5935.02 | 418 ⁴¹ | 5929.84 | 8.7e-04 | Σ _b ⁺ (5945) ⁰ | 5791.90 | 411 ⁴¹ | 5791.80 | 1.8e-05 |
| Λ(1820) | 1820.00 | 127 ¹² | 1821.76 | -9.7e-04 | Λ _b ⁰ (5955) ⁰ | 5952.30 | 422 ⁴² | 5955.31 | -5.1e-04 | Σ _b ⁰ (5955) ⁻ | 5955.33 | 420 ⁴² | 5957.69 | -4.0e-04 |
| Λ(1830) | 1825.00 | 127 ¹² | 1821.76 | 1.8e-03 | Ω _b ⁻ (6227) | 6226.90 | 439 ⁴³ | 6223.67 | 5.2e-04 | Ω _b ⁻ | 6046.10 | 426 ⁴² | 6041.64 | 7.4e-04 |
| Λ(1890) | 1890.00 | 132 ¹³ | 1891.46 | -7.7e-04 | found ok if diff= massPDG - massNuons < 8 MeV, very good if diff < 5 MeV, veryvery good if diff < 1 MeV findall_0.root nparticles = 116093 ==>> nbaryonsPDG = 133, nbfoundok = 133, nbverygood = 111, nbveryverygood = 76 | | | | | | | | | |
| Λ(2100) | 2100.00 | 147 ¹⁴ | 2102.68 | -1.3e-03 | | | | | | | | | | |
| Λ(2110) | 2090.00 | 146 ¹⁴ | 2089.06 | 4.5e-04 | | | | | | | | | | |
| Λ(2350) | 2350.00 | 165 ¹⁶ | 2354.83 | -2.1e-03 | | | | | | | | | | |

Figure 16. PDG baryons masses compared to nuons.

Important Remark 2. When looking at this linearity, one could also think that one should be able to determine this frequency from the PDG tables directly by making a Fourier Transform. Unfortunately, this does not work because there are by definition missing masses (not yet found!). Charged and neutral versions of a particle have substantially different masses, or particles masses like resonances have a large mean error.

4. Charge Density in the Neutron

Building experiments to understand the charge distribution/density in the nucleon has always been a challenge for physicists. The standard way to investigate the internal proton structure has always been via beams of lighter objects (ν, e, μ, π) or e-p collisions. This task is particularly difficult as the interpretation of results depends mainly on the assumed (quark/gluon) model of the proton. For the neutron case the task is even more difficult as it is hard for the time being to realise a e-n or ν, n, π or μ, n collider. In general the understanding of the neutron structure has been made via e, ν, μ beams into deuterium or carbon targets. In this case the estimation of the neutron structure is made by subtracting the *better known* proton results.

However, in 2010 a very interesting experiment BLAST [20] has been conducted at the MIT/BATES accelerator. An electron beam (few GeV) is colliding with a deuterium jet. This experiment has published a very interesting article [20] estimating the charge density inside the neutron. The results show a slightly positive core (max at 0.17e) and a small negative crown vanishing slowly after several fermis. It would be nice to see other experiments confirming this result. This result presents a nice challenge for the nuon model. A simple program npCharge shoots electrons into neutrons taken from a data base of several thousand neutrons generated by the program findall that computes the masses of all particles. The electrons are sent through the neutron at random distances from the centre (as in the experiment) and at each step (40 steps in total) the charge density is estimated. In the left of **Figure 17** one can see the result (black points with errors) and the result from BLAST superimposed (red line). In the right the average charge is shown, and of course, expected to be 0 on average.

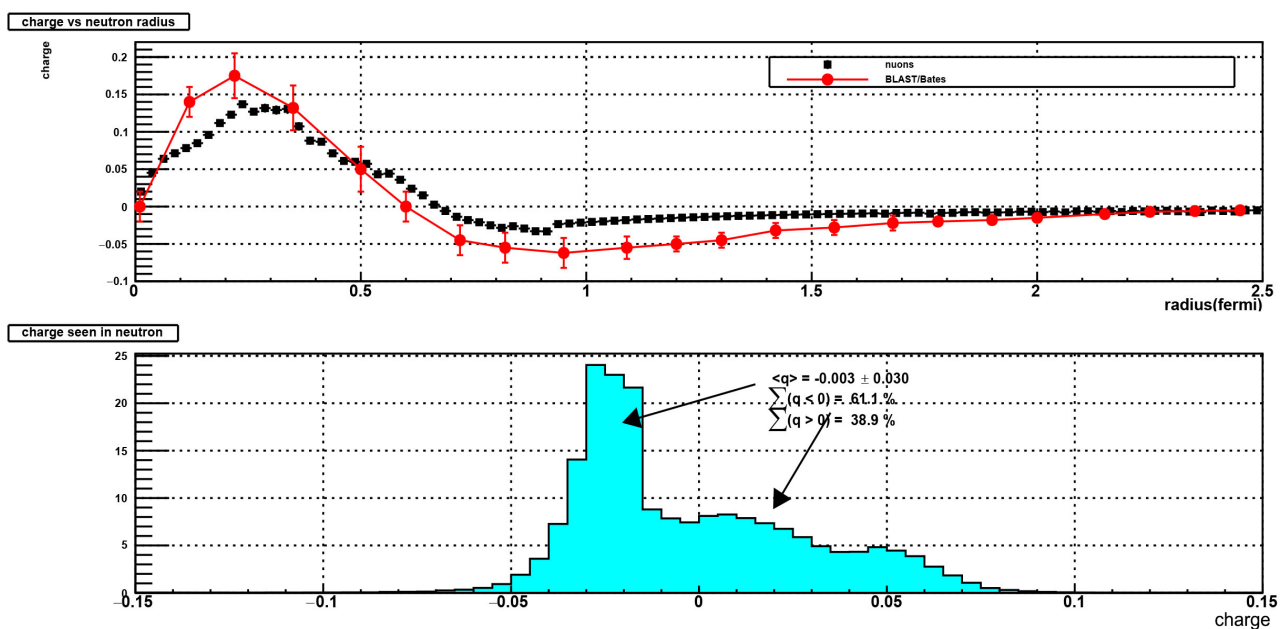


Figure 17. Charge Density vs radius (left). Average charge (right).

5. Testing the Model: Current and Future

In addition to the static tests presented above, the proposed model can be tested with many different experiments with different physics processes and energies. The most obvious tests are with:

- Elastic scattering with proton-proton or proton-antiproton
- Diffraction processes, e.g. proton-proton
- Deep inelastic scattering, e.g. electron-proton
- Highly inelastic collisions with production of jets in proton-proton collisions
- HeavyIons collisions

So far the model has been tested with proton-proton, proton-antiproton elastic scattering, electron-proton, positron-proton deep inelastic scattering and highly inelastic collisions that are described in the following sections.

6. Comparison with p-p and p- \bar{p} Elastic Experiments

p-p and p- \bar{p} elastic scattering experiments offer nice ways to measure the proton/antiproton shape and near surface constituents. Many results have been obtained with collider experiments starting with the ISR [21] up to the recent data with TOTEM [13] at the LHC. The result of these experiments is always shown in terms of the four momentum transfer $t = -p^2\theta^2$. The histogram of t exhibits 3 domains: a first domain for the small values of t that is traditionally interpreted as the Coulomb scattering contribution when the 2 particles do not overlap or are far away. The shape of the t distribution in this area has an exponential behaviour with a very large slope.

The first slope for small values of t is due to the Coulomb forces when the particles do not overlap up to a very large distance $distmax$. Figure 18 shows the maximum radial distance $distmax$ between the 2 protons as a function of the beam energy.

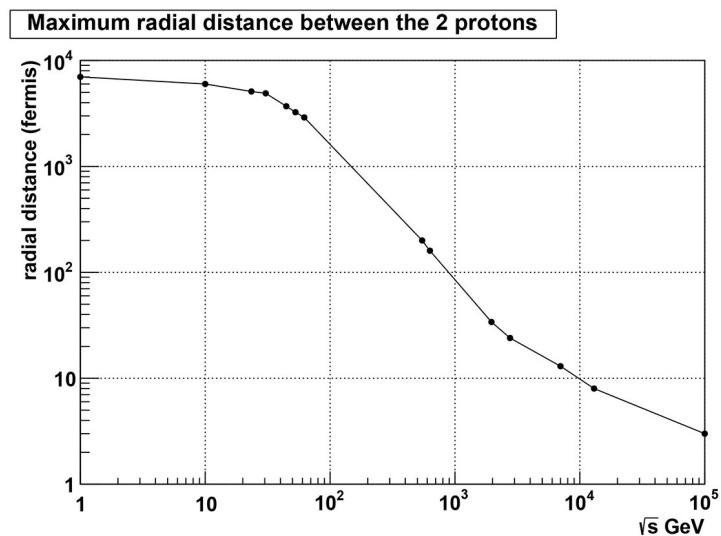


Figure 18. Maximum distance between the 2 protons center.

The large values of t are interpreted via the Strong Force contributions when the 2 particles interpenetrate. The third domain in the middle exhibits a dip and a maximum. The value of t at the dip is in general interpreted as being proportional to the inverse of the proton radius. As the position of the dip decreases when the energy increases, one usually says that the proton radius increases with the energy. The interpretation of the shape of the dip and associated maximum is interpreted via several mechanisms, e.g. the Pomeron-exchange [22] mechanism and Regge trajectories [23].

Using the nuon model, one reproduces extremely well the experimental results for all available data ranging from $\sqrt{s} = 27.43$ GeV at the ISR [21], 536 GeV at SP \bar{P} S [24], 1960 GeV at the Tevatron [25] and 7 and 13 TeV at the LHC [13] (see Figures 19-24). The totem program has been written taking protons at random from the proton data base and colliding them with different impact distances. While the protons move, their internal nuons rotate and the necessary Lorentz transformations are taken into account. For example at 7 TeV, colliding 2 protons is like colliding 2 pancakes since their γ factor is about 3730. It is interesting to note that in the case of proton-antiproton scattering, the dip nearly vanishes in the experimental data and this behaviour is well reproduced by the model.

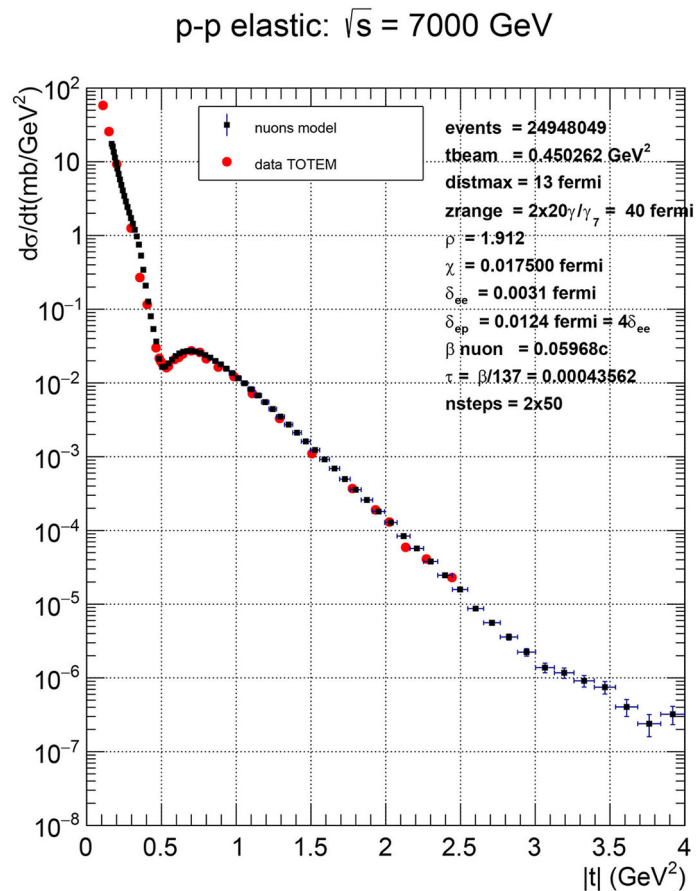


Figure 19. Momentum transfer distribution at LHC 7 TeV TOTEM.

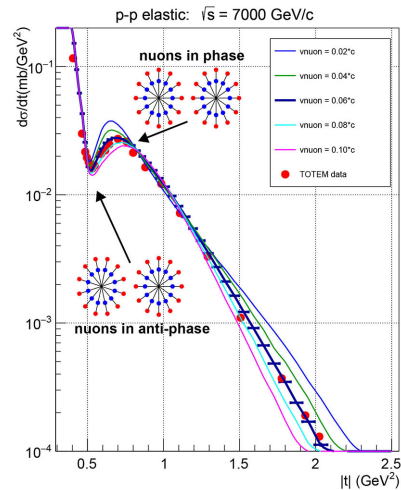


Figure 20. Momentum transfer distribution for various β at 7 TeV.

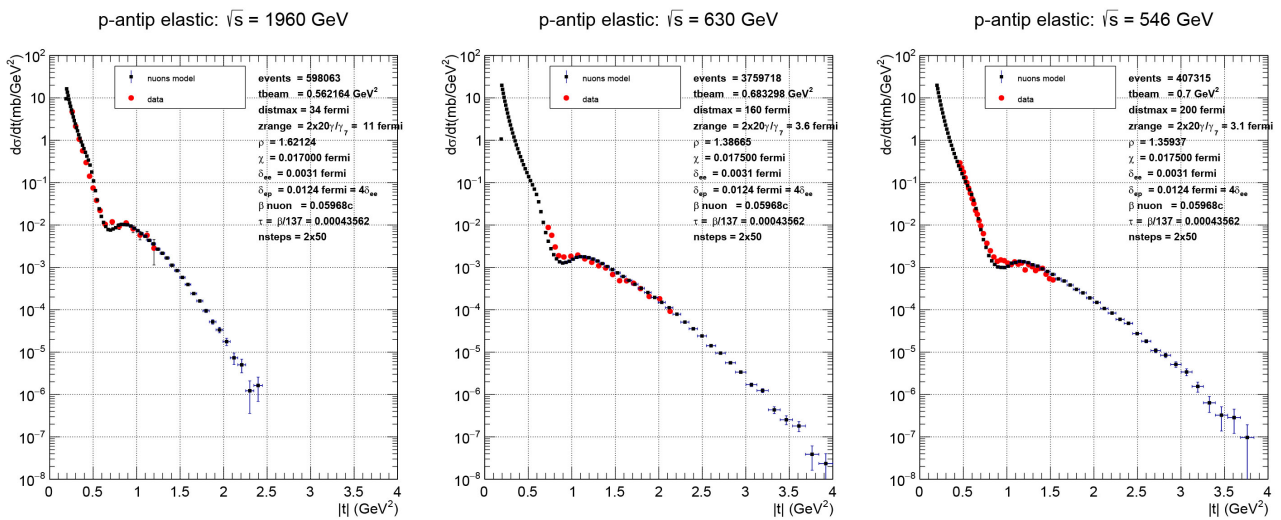


Figure 21. Tevatron (D_0) and SPS (UA4) proton-antiproton elastic scattering.

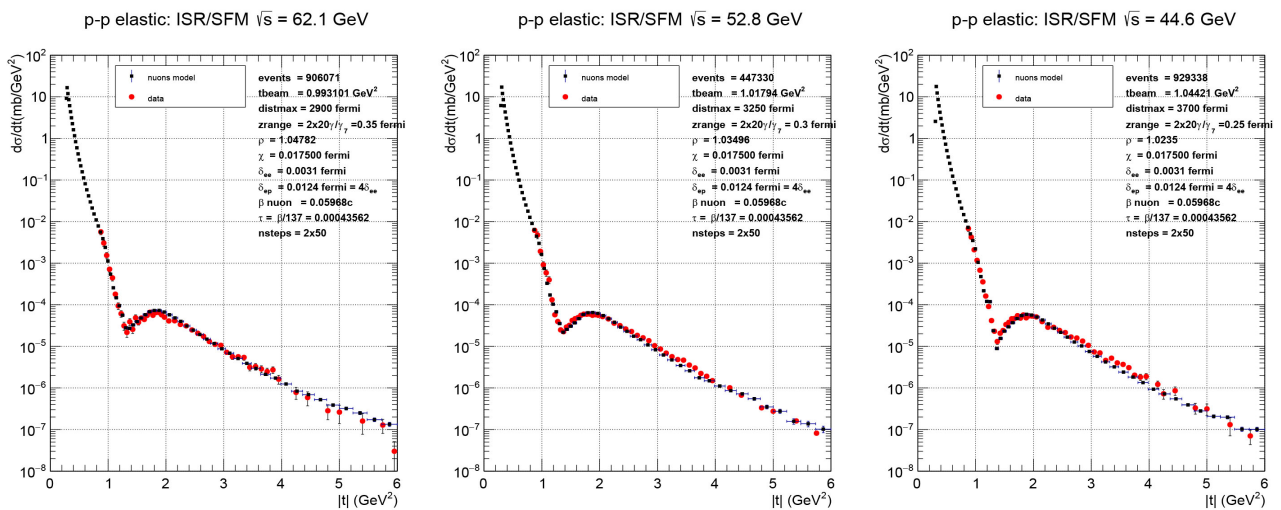


Figure 22. ISR proton-proton elastic scattering from $\sqrt{s} = 62.1 \rightarrow 44.1$ GeV.

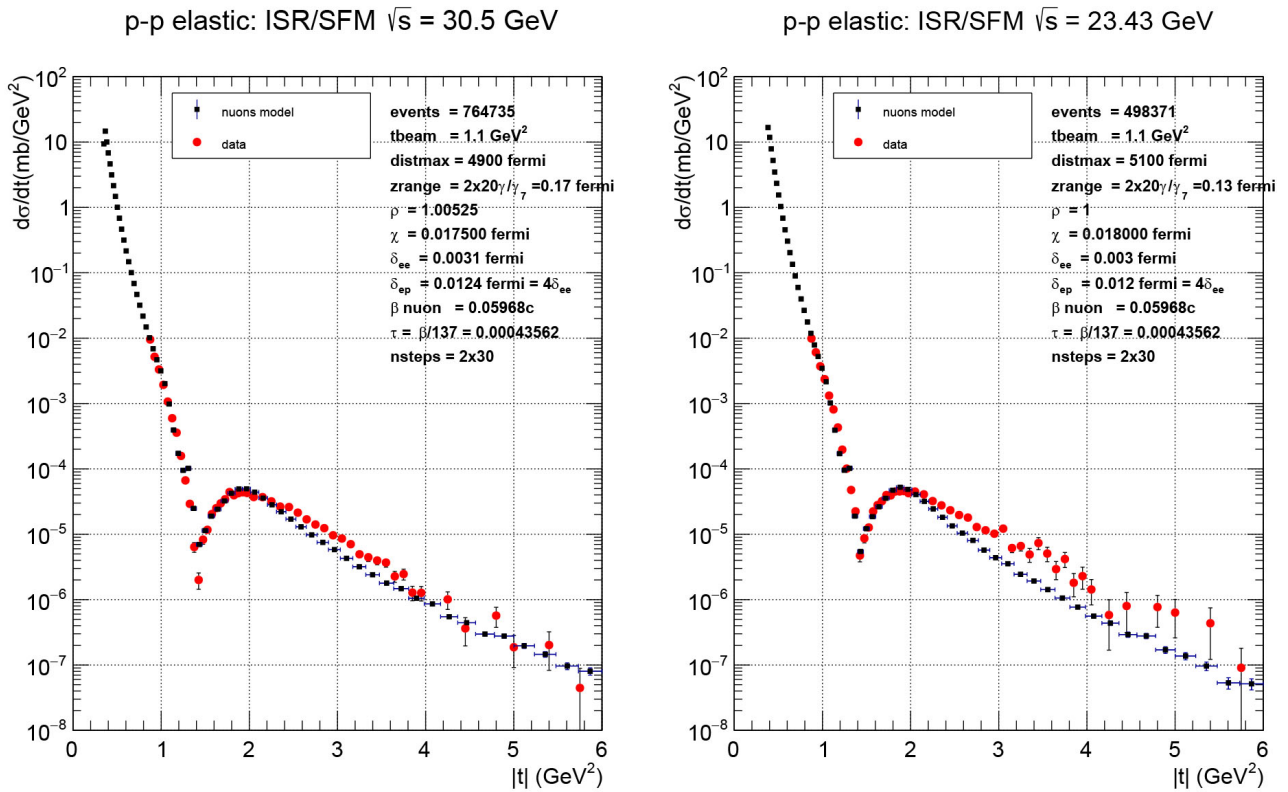


Figure 23. ISR proton-proton elastic scattering from $\sqrt{s} = 30.5 \rightarrow 23.43$ GeV .

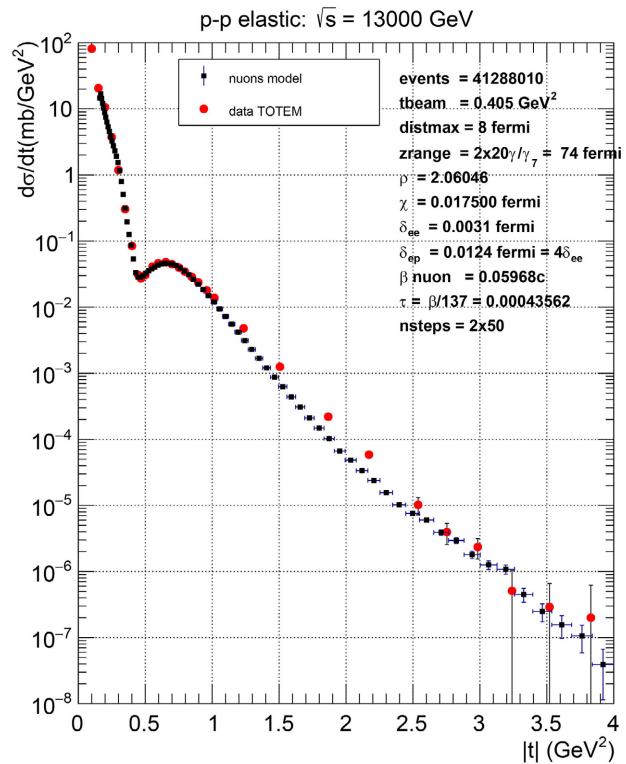


Figure 24. Nuons model prediction for the momentum transfer distribution at LHC 13 TeV compared to the TOTEM results.

The second slope for the high t values is also due to Coulomb interactions when the particles manage to interpenetrate with no destruction. The dip area is the case of the 2 particles tangent or with a very tiny interpenetration. This last case is interesting as we see several contributions generating this dip and maximum. The first contribution is the result of the of the 2 spinning particles and the nuons (such as the spokes of a bike wheel) that can be in phase or anti-phase. The best reproduction of the experimental results is obtained when the nuons are assumed to rotate around the axial nuons at a speed in the range $0.04c < kBeta < 0.10c$. We find that $kBeta = 0.06c$ is the best value for all energies from 21 GeV to 13 TeV. In **Figure 20** we show the effect of varying $kBeta$ between 0.02 and 0.10 in the dip region at 7 TeV. The second major contribution to this dip/maximum is due to the fact that nearly tangent protons are not seen by the trigger of the experiment because the peripheral positrons collide and generate an inelastic interaction. One must also note that the shape of the *dip* is very sensitive to the position of the nuons inside the proton. If one smears the position of these nuons by more than one *millifermi*, about 50 per cent of the *dip* disappears. It would be very interesting to redo the p-p elastic experiments at the ISR energies with improved detector precision. In particular, the study of the precise cross-section around the *dip* region could carry more information about the proton structure.

In **Figure 24** the predictions for the momentum transfer distribution at 13 TeV are presented, compared to the results from TOTEM at 13 TeV.

In **Figure 25** the comparison with many experiments for proton-proton or proton-antiproton scattering ranging from the ISR energies to the latest LHC results.

7. Comparison with LHC p-p Collisions at 900 GeV and 7 TeV

Using the collide program, the case of inelastic collisions at the LHC has been simulated (900 GeV, 2.76 TeV, 7 TeV, 8 TeV and 13 TeV). See References CMS [26], ATLAS [27], ALICE [28]. The program collides protons at random impact distances. This simulation has two phases:

- Hard collisions between very close electrons/positrons in the colliding nuons producing jets. To describe this collision model, we take the average charged particle multiplicity that has been measured in great detail at the various e^+e^- colliders. For this work we have taken the parameters by P. V. Shlyapnikov [29] in the form $nch = 2.80829 - 0.518406 * \sqrt{sn} + 1.00586 * sn$ where sn is the center of mass energy available in the collision of electron/positrons from the 2 colliding nuons. The program generates a collision only when the distance $d12$ between the nuon components is less than a parameter $d12min$ that is around 0.1 fermi for collisions at 7 TeV, *i.e.* about 6 per cent of the proton radius. $d12min$ is about constant with the collision energy and represents the transversal move of a nuon rotating at about 0.06c when the proton travels about 1 fermi. The 3 cases described earlier (axial-axial, axial-radial and radial-radial) are processed with specific algorithms (see example in **Figure 26**).

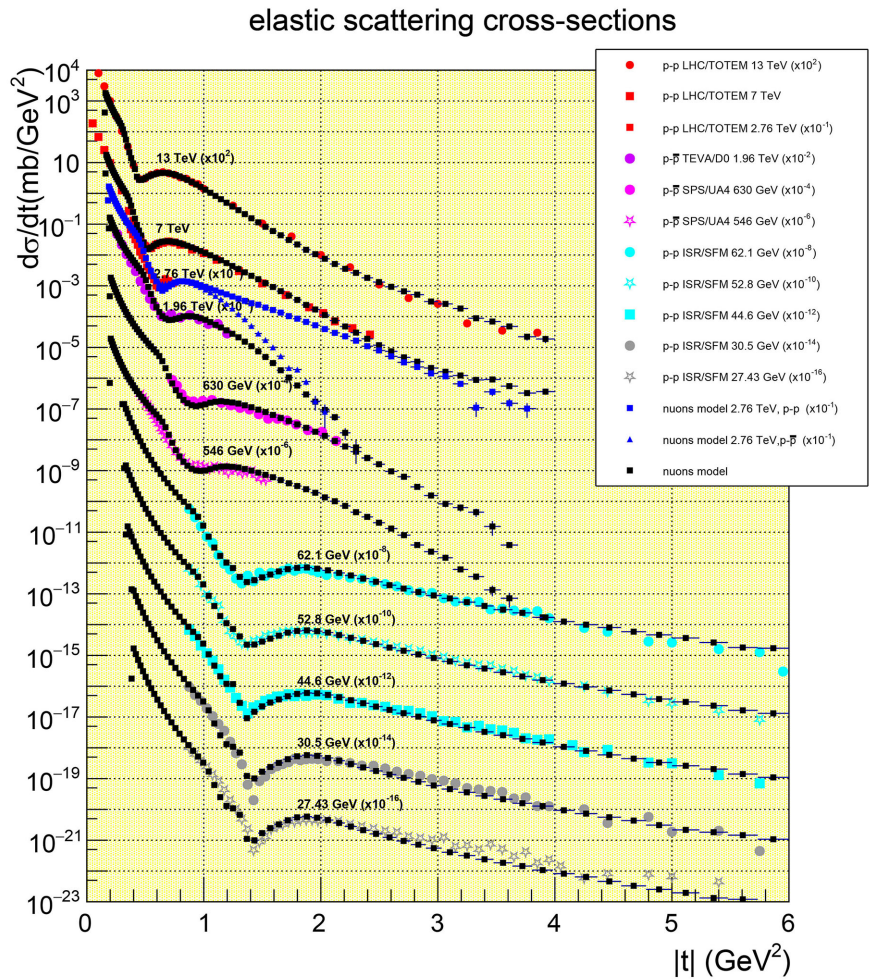


Figure 25. Nuons model compared to many experiments in a wide energy range.

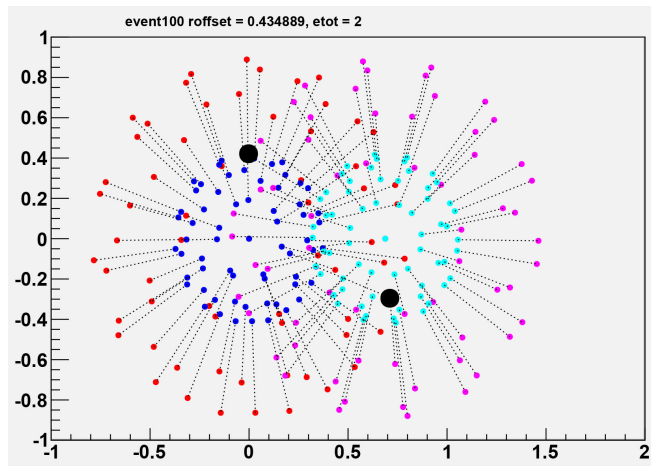


Figure 26. Example of p-p collision showing 2 colliding nuons.

In radial-radial collisions the corresponding collision energy is assumed to be 2 times the electron energy divided by $d12$ when the electrons rotate in the same direction or 0.5 times the electron energy divided by $d12$ otherwise.

In axial-radial collisions the collision energy is assumed to be $0.5 \cdot \max Pt$ times the value of the Gaussian with $\sigma = kBeta$ at a distance $d/2$.

In axial-axial collisions the collision energy is assumed to be $\max Pt$ * (the product of the two electron/positron gaussians of standard deviation *electron-Sigma* at a distance $d/2$). The high Pt tracks and jets are generated by axial-axial collisions. If one smears the position of the axial nuons by just a few millifermi, then the high Pt tracks are not generated anymore (eg. no tracks with $Pt > 80$ GeV/c for 7 TeV collisions).

- Soft collisions happening between the nuons left after all hard nuon collisions have been processed. When the original particle is destroyed the remaining nuons are candidates for a recombination. A hadronization model is included in the program to build particles such as $\mu, \pi, K, \eta, \rho, \phi, p, \Lambda, \Sigma, \Xi, \Omega$ with these remaining nuons.

We can also compare the ratio of soft to hard events with the experimental data or other Monte-Carlo systems. In a recent Alice paper [30] the ratio *soft/hard* events is indicated for 3 energies (see **Table 1**). An event is classified as soft when no tracks with a $P_t > 2$ GeV/c is found in the range $-0.8 < \eta < 0.8$.

As shown in **Figures 27-30**, the P_t and η distributions are extremely well described by the model. Many additional plots are also available showing the good agreement for the number of generated particles, or distributions such as the ratios $\pi/p, K/p$. In **Figure 31** the predictions at 13 TeV for the charged particle Pt distribution (top) and multiplicity distribution (bottom) are presented, compared to the results from CMS and ATLAS.

8. Particles Pt Distribution Peculiarities

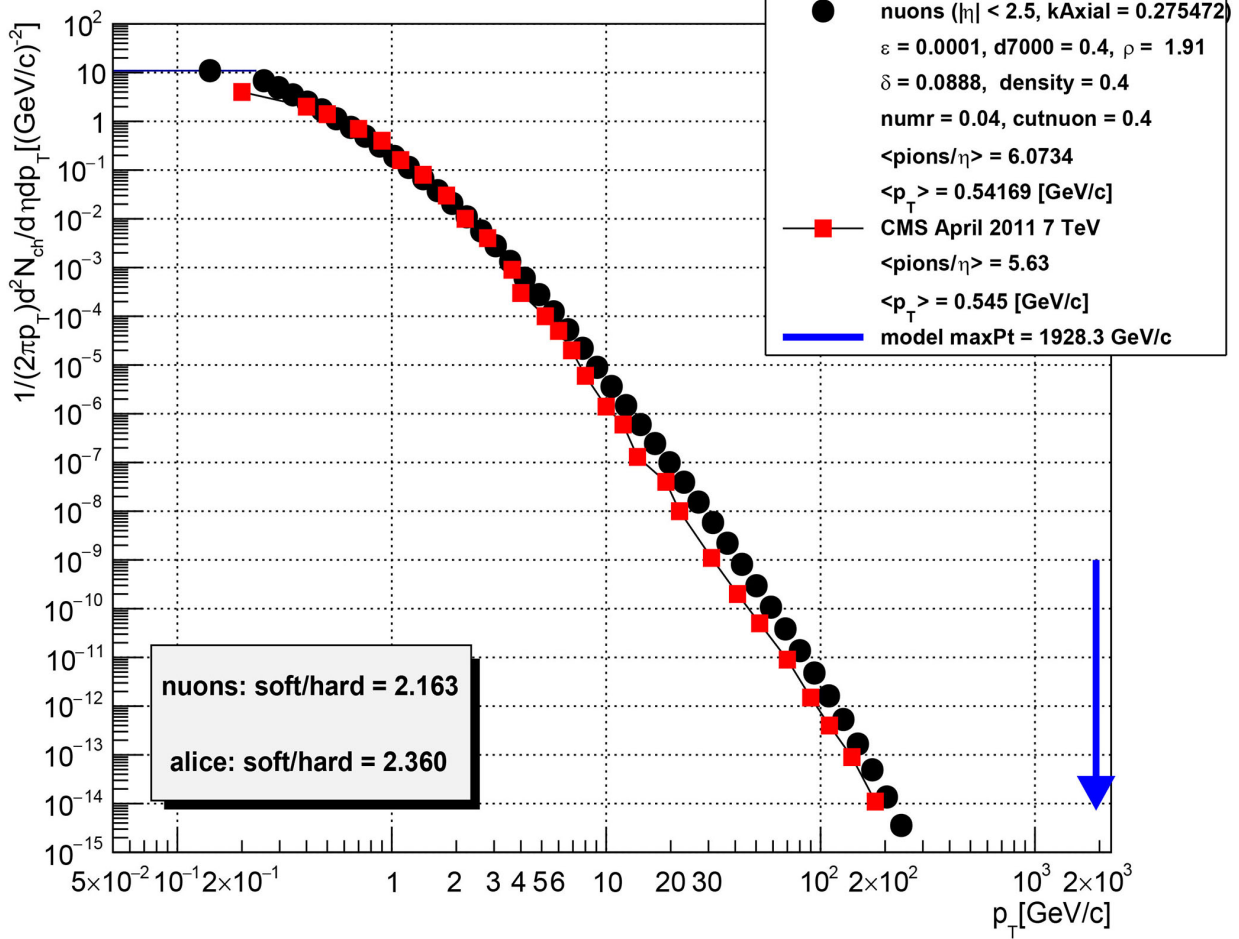
The Particles Pt distribution was traditionally modeled with a power law with one single slope as a function of Pt. However with the recent LHC high statistics results, it is clear the slope of the power law changes drastically with Pt. In **Figure 32** left we compare the slope as a function of particles Pt at 7 TeV with the CMS data and the predictions from Pythia8 and the NUONs model.

In **Figure 32** right, we show the predictions of the NUONs model for the ratio of the Pt distribution divided by the Pt distribution for minimum bias events as a function of the event multiplicity.

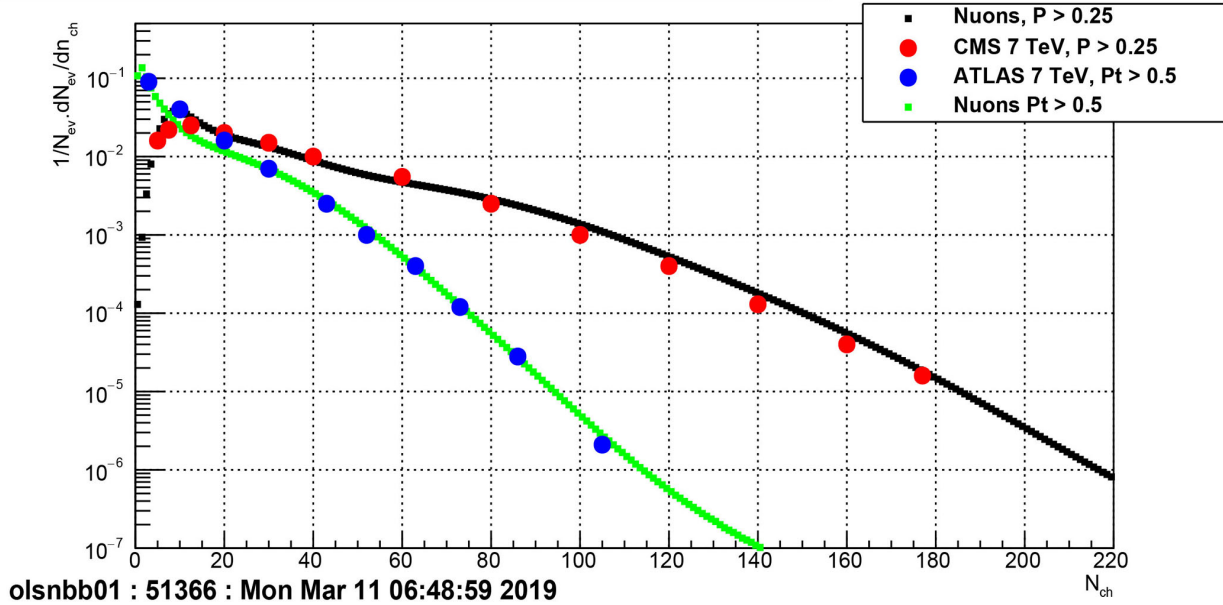
Table 1. Ratio of the number “soft” to “hard” events for ALICE data, the nuon model and MC generators.

| | 0.9 TeV | 2.76 TeV | 7 TeV |
|--------------|-------------|-------------|-------------|
| ALICE (data) | 5.70 | 3.54 | 2.36 |
| NUONS | 5.84 | 3.16 | 2.03 |
| PHOJET | 8.53 | 4.34 | 2.52 |
| PERUGIA-0 | 5.6 | 3.26 | 2.06 |
| PERUGIA-2011 | 6.78 | 3.64 | 2.29 |
| PYTHIA8 | 7.28 | 3.92 | 2.37 |

$\sqrt{s} = 7000 \text{ GeV}/c^2 : 13038107331 \text{ events}$



Charged particles multiplicity, see: cms_jhep.01.2011.079.pdf



olsnbb01 : 51366 : Mon Mar 11 06:48:59 2019

Figure 27. Pt and particle multiplicity distributions at 900 GeV compared with CMS results.

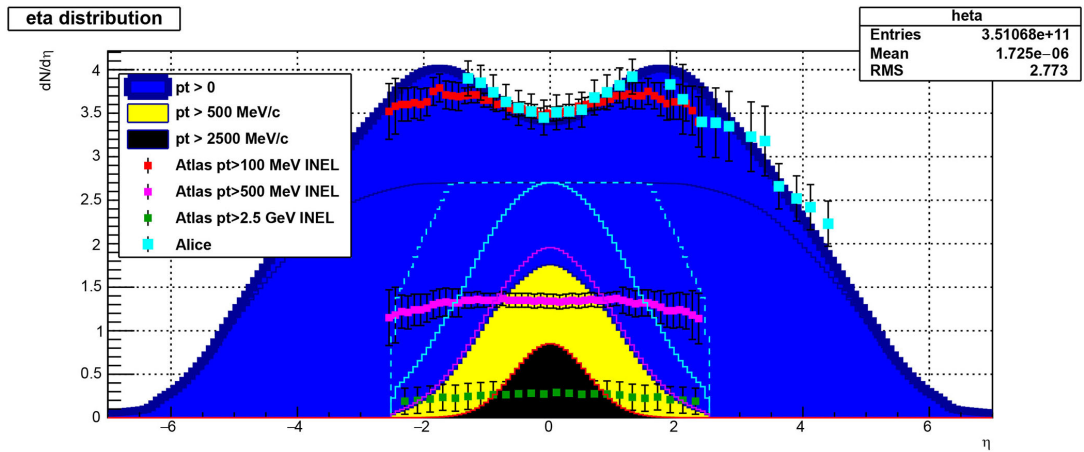


Figure 28. Pseudo-rapidity at 900 GeV compared with LHC results.

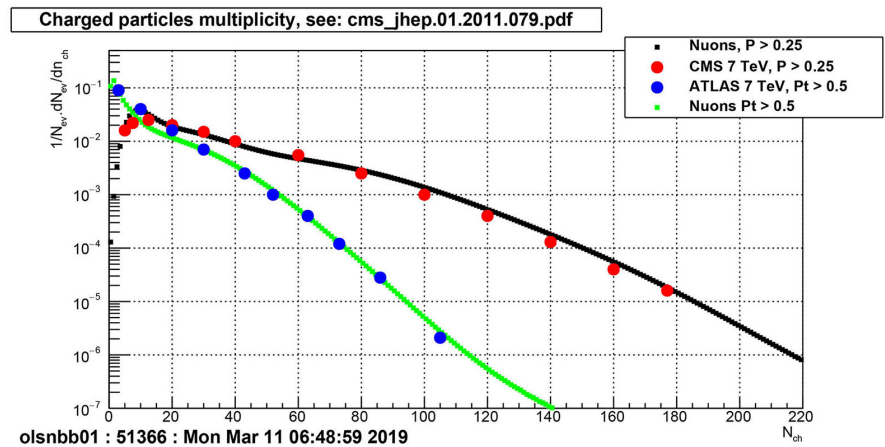
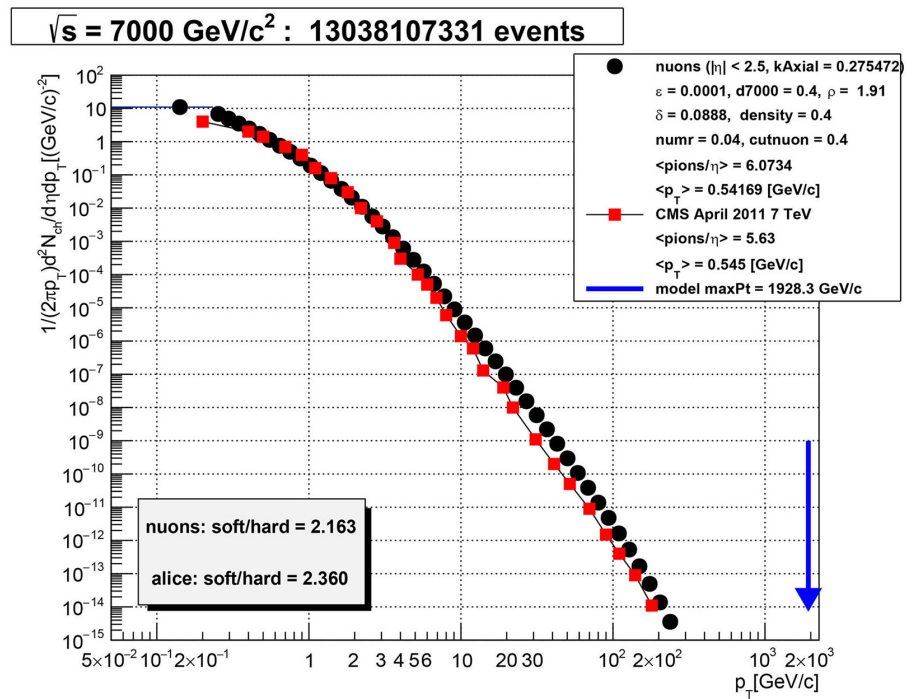


Figure 29. Pt and particle multiplicity distributions at 7 TeV compared with CMS results.

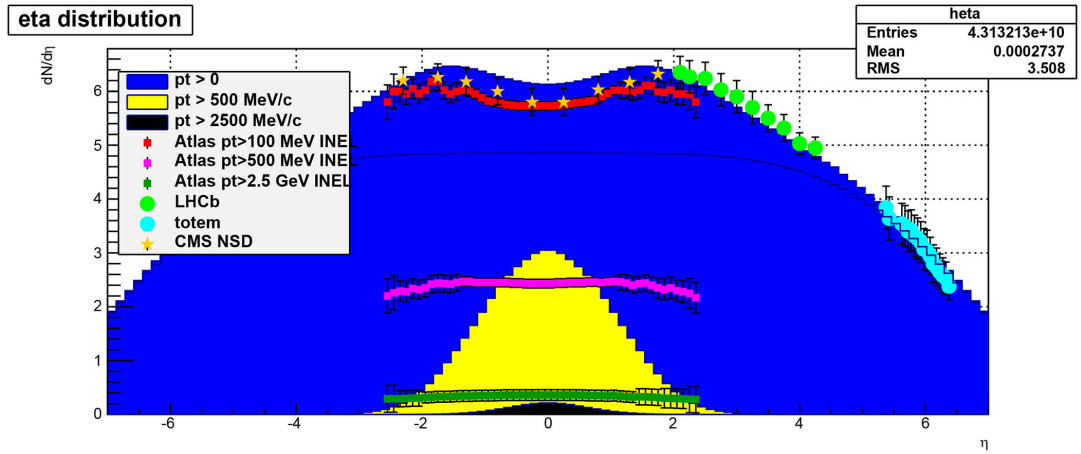


Figure 30. Pseudo-rapidity distribution at 7 TeV compared with LHC results.

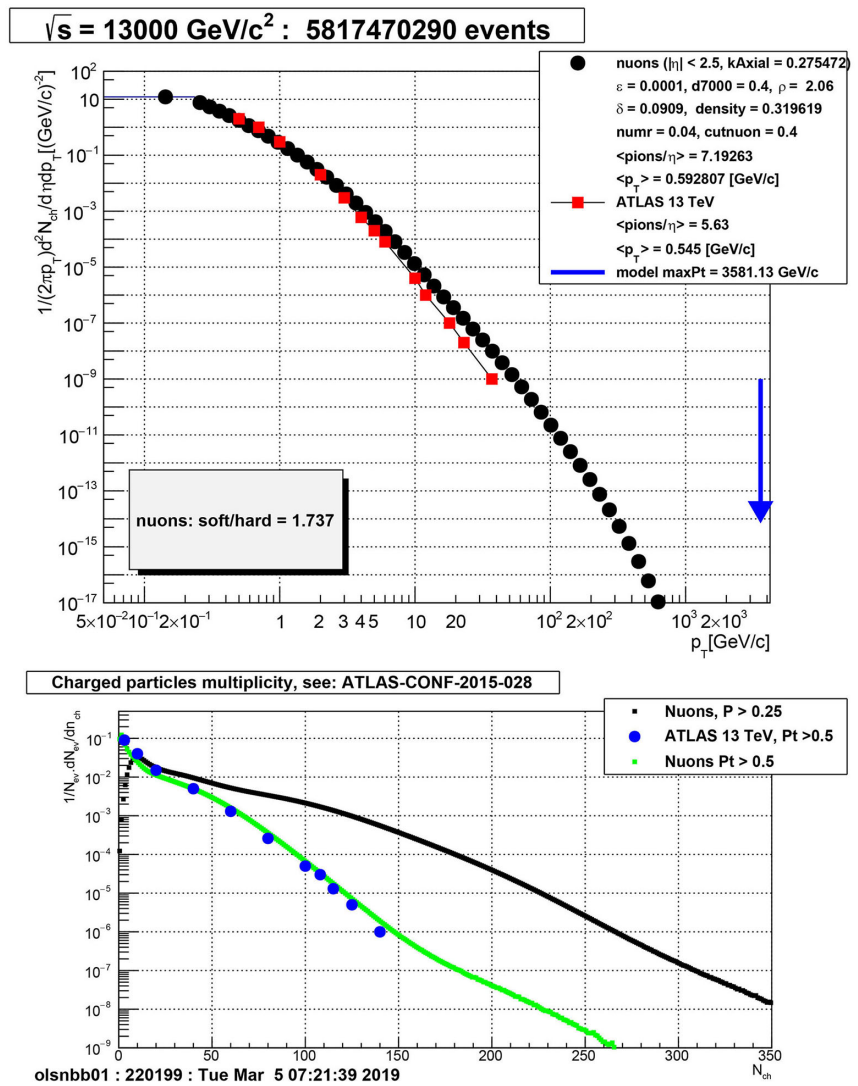
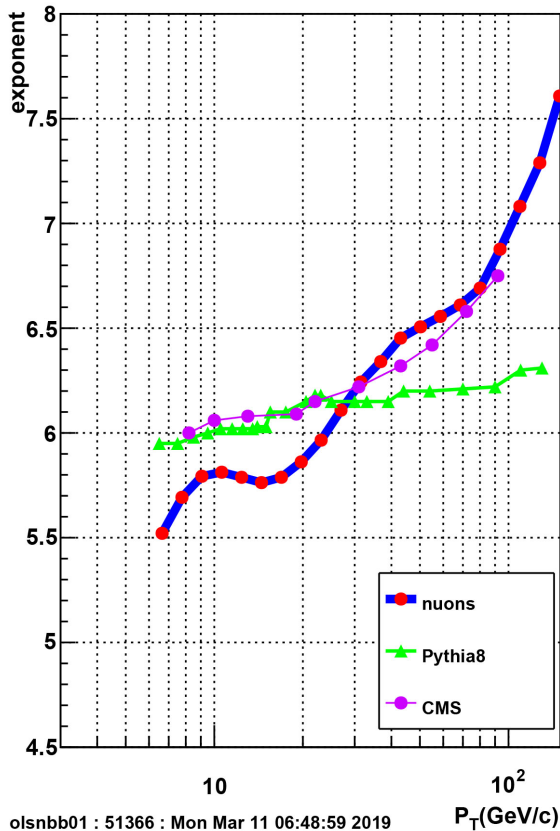


Figure 31. Nuons model predictions at 13 TeV for the charged particle Pt distribution (top) and multiplicity distribution (bottom) are presented, compared to the results from CMS [31] and ATLAS [32].

exponent of power law fit vs Pt, $\sqrt{s}=7000$, $|\eta| < 2.5$



Pt vs multiplicity families, $\sqrt{s}=7000$, $|\eta| < 2.5$

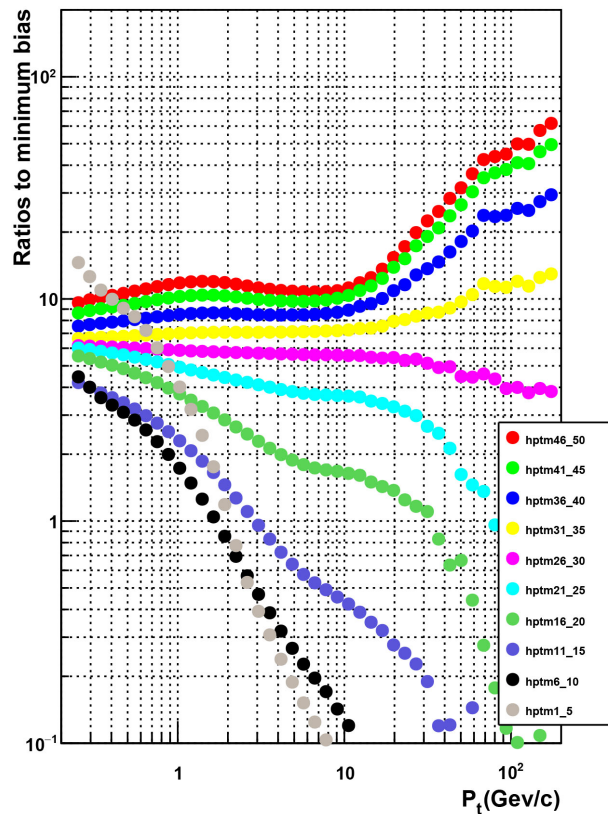


Figure 32. Left: Particles Pt cross-section slope compared with CMS results and Pythia8. Right: Particles Pt distribution divided by minimum bias Pt distribution for several event multiplicities.

While doing comparisons with many experimental data at various energies, one of the conclusions has been the lack of some variables facilitating the task. In the same way that in deep inelastic experiments, the Bjorken x variable had been introduced in the early days, it is proposed to introduce two new variables representing respectively the fraction of the event energy carried by one particle and the measured event energy:

$$Xt = 2Pt/\sqrt{s} \quad \text{and} \quad Xtev = \sqrt{\Sigma P^2_t}/\sqrt{s}$$

Using the two variables, one can now produce distributions like the one shown in **Figure 33** where interesting shapes can be seen for the high values of $Xtev$. See the dip in the cross-section vs Xt for the 2 bottom curves $xtev$ [0.051, 0.12] and $xtev$ [0.12, 0.28]. It would be interesting to read a confirmation from the LHC experiments.

9. Jets Distribution at the LHC

Using the collide program one can investigate the jets distribution in p-p collisions at 7 TeV at the LHC. The program considers that a jet is produced whenever the distance between the electron and positron of 2 colliding nuons is less

than $d12min = 0.08$ fermi (ie the hard collision parameter described above), the jet Pt above PtjetMin and the multiplicity above a threshold (e.g. 8 charged particles at 7 TeV). Multiple nuon collisions may happen (Multiple Parton Interactions) in a given proton proton collision, each one generating 1, 2 or more jets. **Figure 34** illustrates one event with 2 jets generated by the collision of 2 axial nuons.

Xt distribution for various values of Xtev, $\sqrt{s}=7000$, $|\eta| < 2.5$, nEvents=2.27934e+09

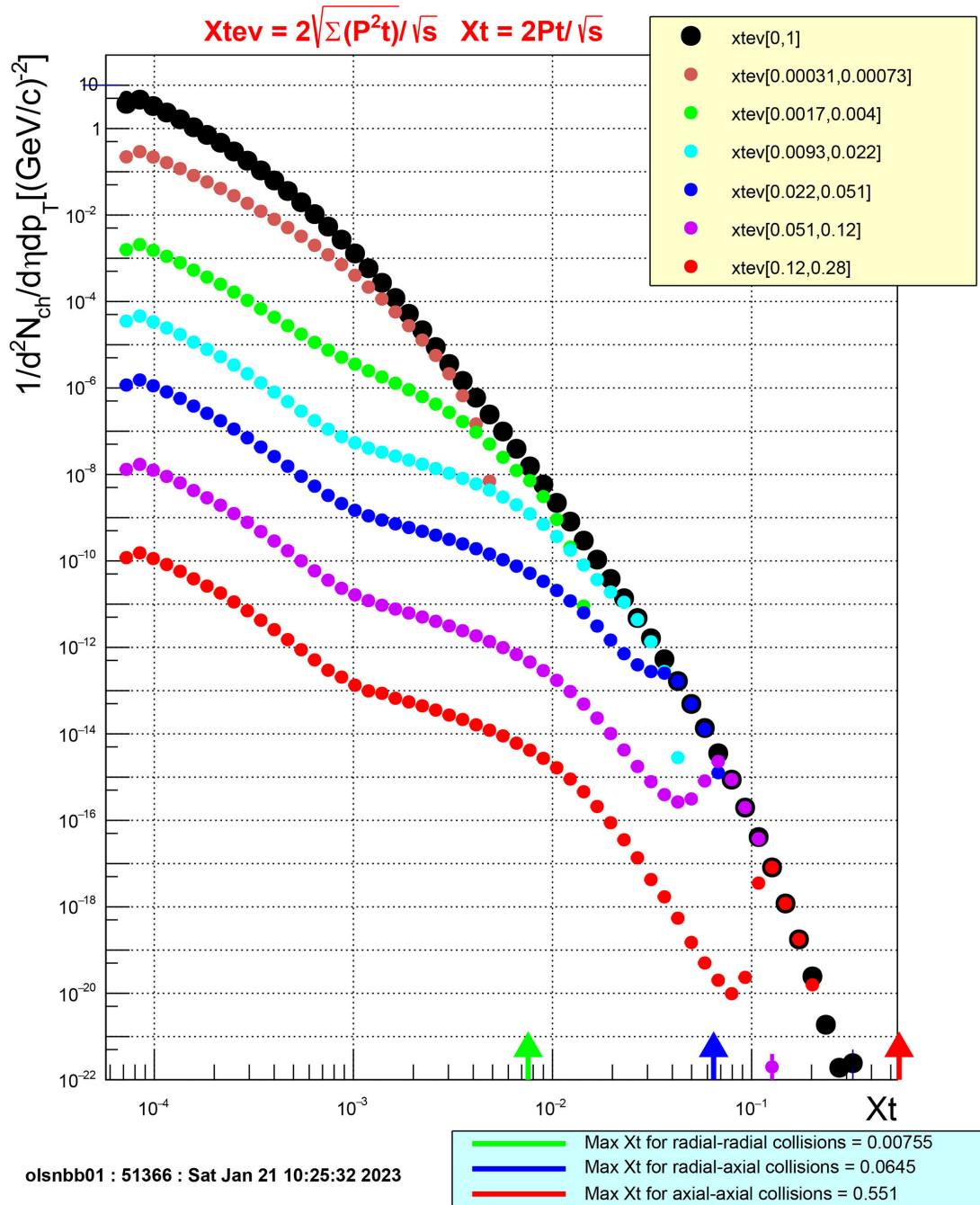


Figure 33. Left: Particles X_t cross-section for different values of X_{tev} .

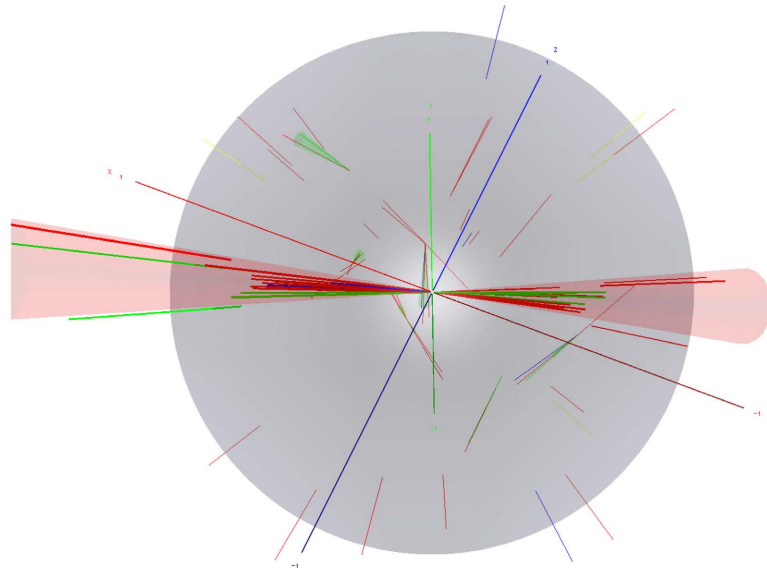


Figure 34. A 2-jet event generated by the collision of 2 axial nuons.

Figure 35 shows the inclusive Jet Multiplicity with the ratio of the n jet cross section to the $(n-1)$ jet cross-section compared to the ATLAS results [27].

Figure 36 shows various jets properties compared to results from CMS [33]. The distributions of jet p_t , average p_t of charged particles belonging to the underlying event or to jets, jet rates, and jet shapes are presented as functions of $N[\text{ch}]$ and compared to the predictions of event generators. The CMS jet reconstruction requires tracks with $P_t > 0.25 \text{ GeV}/c$, $-2.4 < \eta < 2.4$, and a trigger condition with at least one track with $-4.65 < \eta_1 < -3.32$ and a track with $3.32 < \eta_2 < 4.65$. In the table only the results with Pythia6 tune Z2 are shown.

In **Figure 37** the jets inclusive P_t distribution (top) and 1st, 2nd, 3rd, 4th leading jet P_t distribution (bottom) are presented, compared to the results from ATLAS and CMS at 13 TeV.

In **Figure 38** the jets inclusive P_t distribution are compared to experimental results at energies ranging from 45 GeV to 13 TeV.

Using the same very low cuts as in the case used for the comparison with CMS [31], the **Figure 39** shows the number of collisions of different types per event as a function of the charged particles multiplicity. This plot may be compared with experimental results investigating Multiple Parton Interactions (MPI) versus the event multiplicity. For the medium and high multiplicity events, most collisions producing jets are from electron-electron radial collisions. All high multiplicity events have an axial-axial nuons collision. When running the program at different energies, one observes that the maximum number of collisions seems to reach a maximum value around 30. **Figure 40** shows (in linear scale in left pad) the number of collisions versus the particle multiplicity for different collision energies (from 900 GeV to 100 TeV). This plot indicates that the number of collisions is proportional to the multiplicity. The pad at the right of the same Figure shows the probability of having N collisions (MPI) per event.

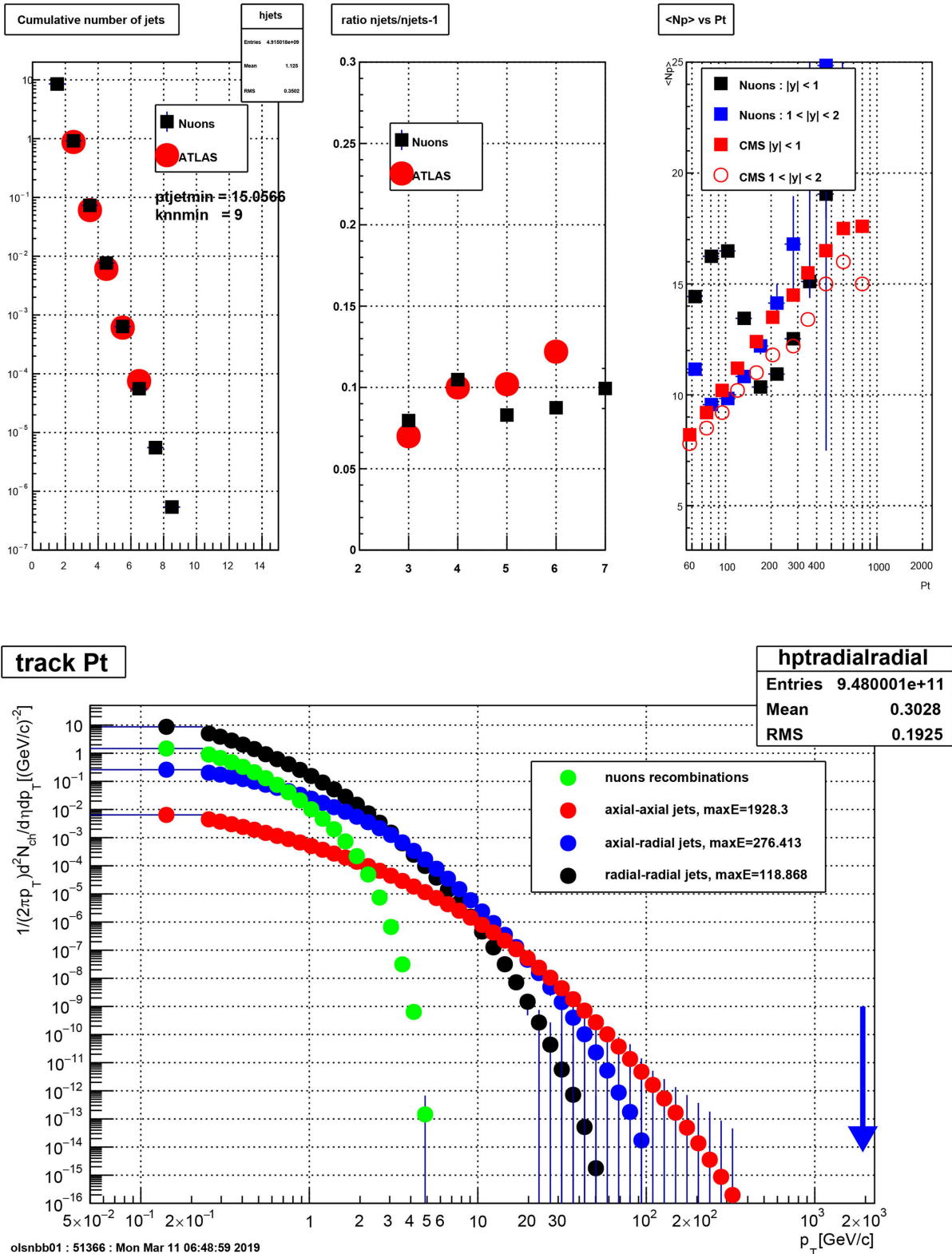


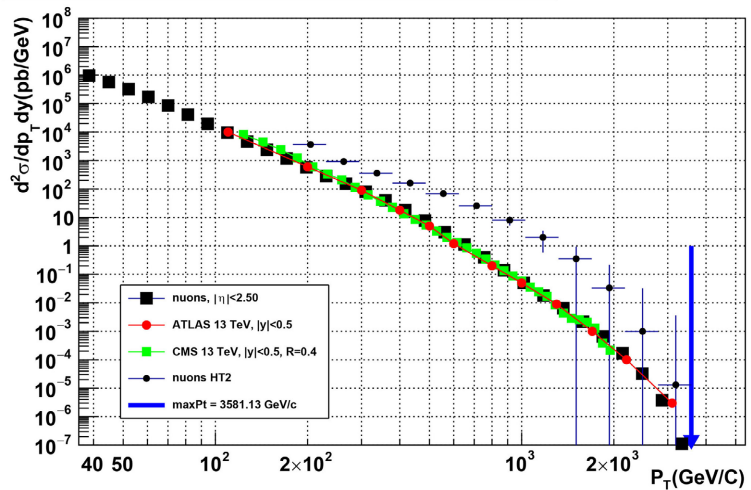
Figure 35. Jets with the Nuons model: Top left: Inclusive number of jets compared to ATLAS data. Top center: ratio 3/2, 4/3, 5/4, 6/5 compared to ATLAS. Top right: Average number of particles per jet as a function of the Pt of the jet compared to CMS data. The picture at the bottom shows the differential cross-section of charged particles versus Pt with a stack of the different contributions.

Jets compared to CMS data at $\sqrt{s} = 7000 \text{ GeV}/c^2$: 13038107331 events

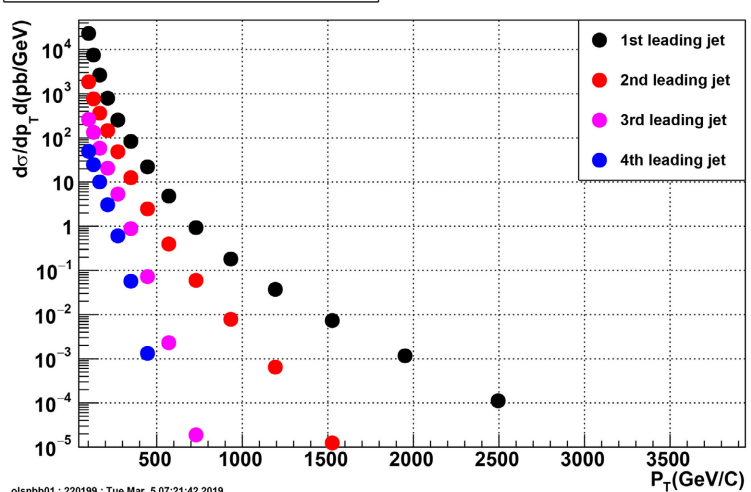
| | | $10 < N_{ch} \leq 30$ | $30 < N_{ch} \leq 50$ | $50 < N_{ch} \leq 80$ | $80 < N_{ch} \leq 110$ | $110 < N_{ch} \leq 140$ |
|---------------------|-----------|------------------------|------------------------|------------------------|------------------------|-------------------------|
| events % | data | 58.10 | 26.40 | 13.00 | 2.19 | 0.24 |
| | nuon | 57.49 | 25.83 | 14.36 | 2.12 | 0.19 |
| p_T^{ch} particle | data | 0.68 ± 0.01 | 0.75 ± 0.01 | 0.80 ± 0.01 | 0.85 ± 0.01 | 0.88 ± 0.01 |
| | nuon | 0.67 | 0.80 | 0.82 | 0.84 | 0.88 |
| | pythia6Z2 | 0.67 | 0.74 | 0.80 | 0.85 | 0.90 |
| p_T^{UE} | data | 0.65 ± 0.01 | 0.71 ± 0.01 | 0.74 ± 0.01 | 0.76 ± 0.01 | 0.77 ± 0.01 |
| | nuon | 0.65 | 0.78 | 0.80 | 0.83 | 0.87 |
| | pythia6Z2 | 0.65 | 0.70 | 0.74 | 0.76 | 0.77 |
| p_T^{ij} | data | 1.90 ± 0.02 | 1.64 ± 0.02 | 1.45 ± 0.01 | 1.32 ± 0.01 | 1.24 ± 0.01 |
| | nuon | 2.23 | 1.85 | 1.77 | 1.77 | 1.54 |
| | pythia6Z2 | 1.86 | 1.62 | 1.44 | 1.33 | 1.29 |
| p_T^{jj} | data | 3.65 ± 0.05 | 3.37 ± 0.04 | 3.15 ± 0.03 | 2.96 ± 0.03 | 2.86 ± 0.03 |
| | nuon | 3.61 | 3.24 | 3.12 | 3.12 | 2.87 |
| | pythia6Z2 | 3.59 | 3.33 | 3.10 | 2.97 | 3.05 |
| $p_T^{ch,jet}$ | data | 6.85 ± 0.06 | 7.04 ± 0.09 | 7.18 ± 0.09 | 7.46 ± 0.11 | 7.81 ± 0.10 |
| | nuon | 7.44 | 7.78 | 7.62 | 7.74 | 8.09 |
| | pythia6Z2 | 7.01 | 7.20 | 7.30 | 7.64 | 8.15 |
| ch.jets/event | data | 0.054 ± 0.004 | 0.287 ± 0.014 | 0.84 ± 0.03 | 2.13 ± 0.09 | 3.68 ± 0.15 |
| | nuon | 0.089 | 0.265 | 0.465 | 0.777 | 0.869 |
| | pythia6Z2 | 0.067 | 0.304 | 0.87 | 2.12 | 3.95 |
| ch.jets/event | data | $(3.2 \pm 0.5)10^{-5}$ | $(3.4 \pm 0.4)10^{-4}$ | $(1.5 \pm 0.1)10^{-3}$ | $(4.3 \pm 0.4)10^{-3}$ | $(1.0 \pm 0.1)10^{-2}$ |
| | nuon | $(8.5 \pm 0.0)10^{-5}$ | $(6.6 \pm 0.0)10^{-4}$ | $(1.0 \pm 0.0)10^{-3}$ | $(3.4 \pm 0.0)10^{-3}$ | $(1.0 \pm 0.0)10^{-2}$ |
| | pythia6Z2 | $(2.7 \pm 0.3)10^{-5}$ | $(3.5 \pm 0.2)10^{-4}$ | $(1.4 \pm 0.2)10^{-3}$ | $(5.7 \pm 0.4)10^{-3}$ | $(2.1 \pm 0.1)10^{-2}$ |

Figure 36. Jets with the Nuons model compared to CMS data.

Jets Pt, $\sqrt{s} = 13000 \text{ GeV}/c^2$: 5817470290 events



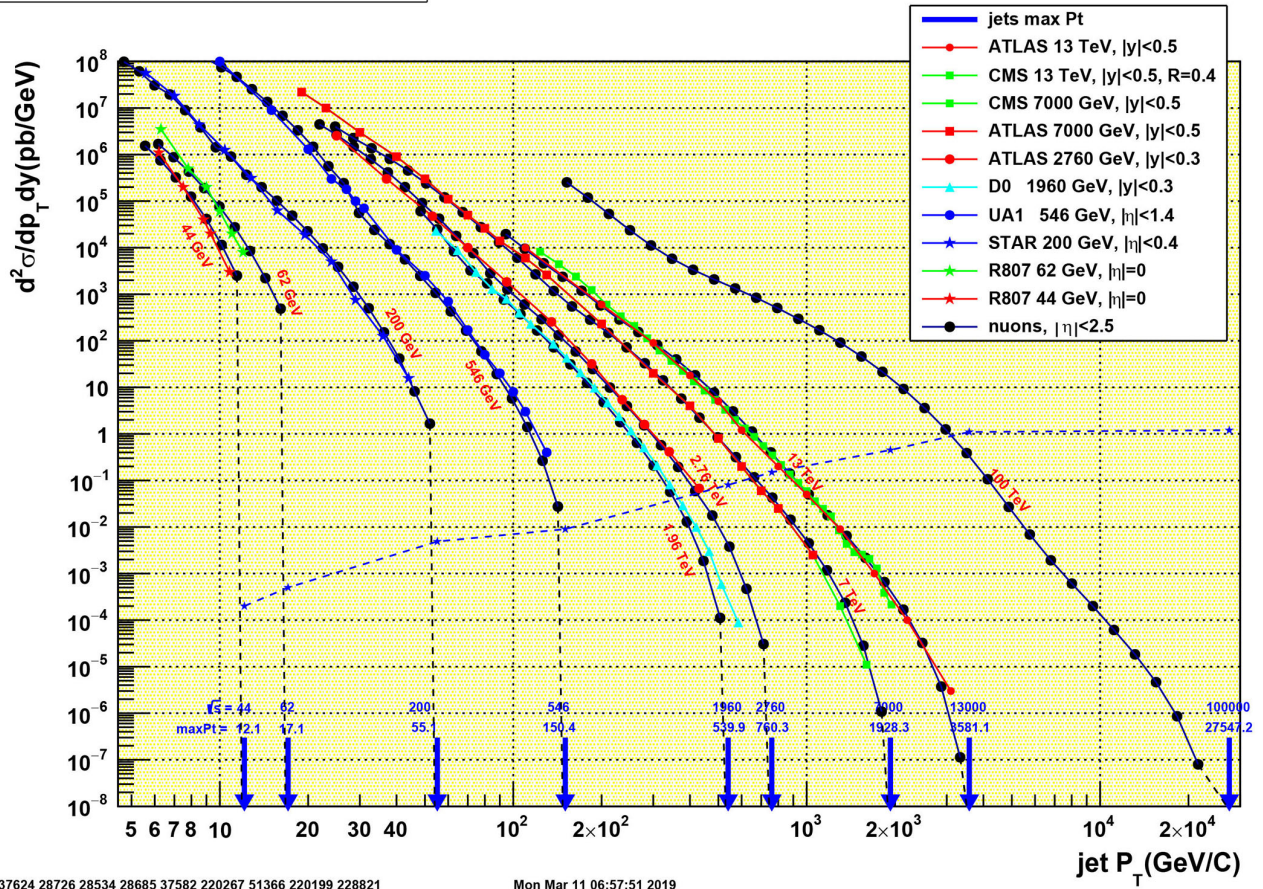
Leading jets, $\sqrt{s} = 13000 \text{ GeV}/c^2$



olsnb01 : 220199 - Tue Mar 5 07:21:42 2019

Figure 37. Nuons model predictions at 13 TeV for the charged particle Pt distribution (top) and multiplicity distribution (bottom) are presented, compared to the results from ATLAS and CMS at 13 TeV.

Inclusive Jets Pt: nuons vs data

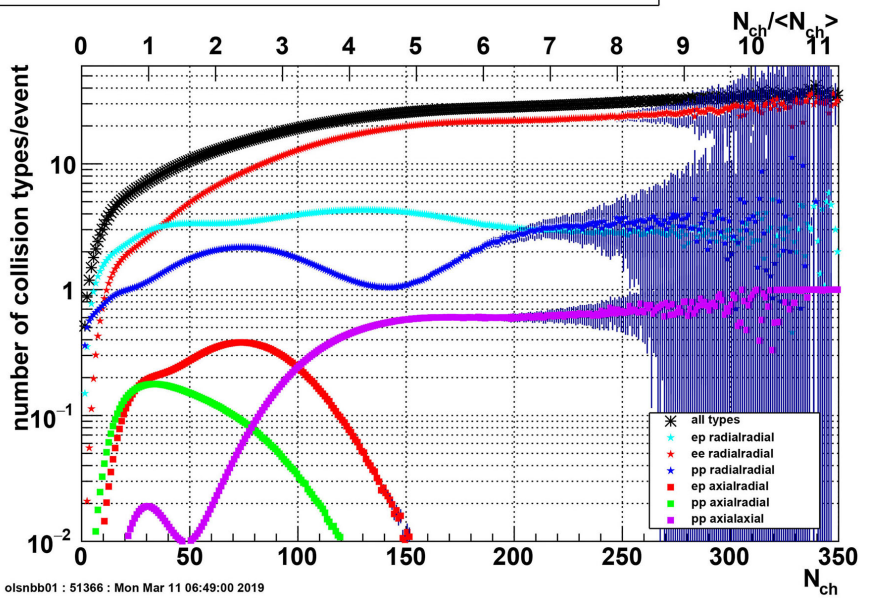


37624 28726 28534 28685 37582 220267 51366 220199 228821

Mon Mar 11 06:57:51 2019

Figure 38. Nuons model predictions compared to experimental results at energies ranging from 45 GeV to 13 TeV. The arrows show the predictions for the jets Pt cut off.

Number of collision types vs $\langle n_{ch} \rangle$ at $\sqrt{s} = 7000 \text{ GeV}/c^2$: 13038108590 events



olsnbb01 : 51366 : Mon Mar 11 06:49:00 2019

Figure 39. Number of collision types per event vs multiplicity at 7 TeV.

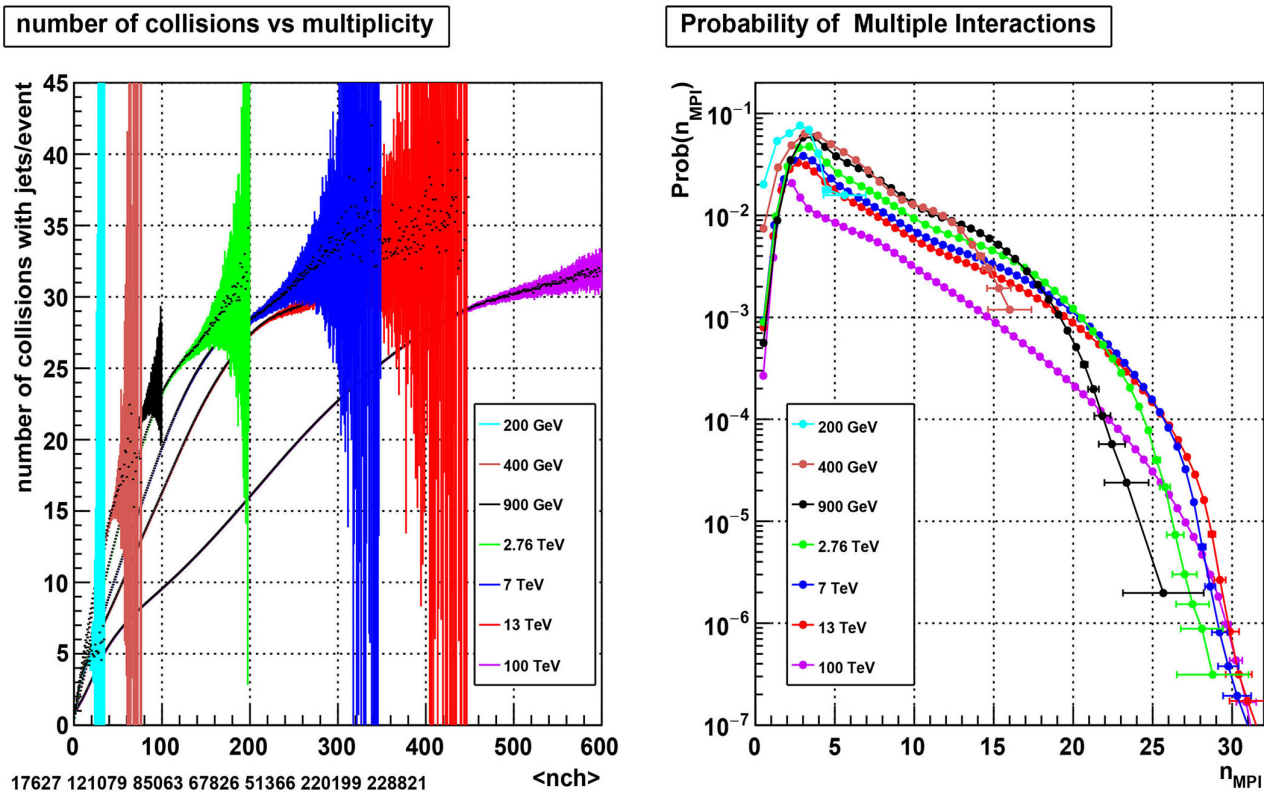


Figure 40. Left: Number of collisions per event vs multiplicity for different collision energies. Right: Probability for an event with N collisions.

10. Comparison with Electron-Proton and Positron-Proton Deep Elastic Experiments at HERA

Using the deep program, a variant of collide, the case of deep inelastic collisions at HERA has been simulated. The incoming electron or positron collides with one or more radial or axial components of the proton. The incoming electron or positron is generated at a distance d with the proton centre and progress step by step inside the proton with a sum of scattering angles depending on the distance with proton components. If the incoming particle survives NC (Neutral Current case), the Q^2 value is computed following the scattering angle. Otherwise CC (Charged Current case) the Q^2 value is computed following the guidelines in the HERA [14] paper summarizing the combined results from the *H1* and *ZEUS* collaborations. The Charged Current case is triggered when the collision distance with one of the electrons or positrons of the proton is less than a distance σ_{CC} equal to 2 micro-fermi.

Since we are dealing with very high Q^2 values, they correspond to the incoming particle (electron or positron) very close to the proton center. In this area, an incoming electron will see 3 attractive positrons and 2 repulsive electrons, and an incoming positron will see 3 repulsive positrons and 2 attractive electrons, see **Figure 41**. This simple fact explains by itself the difference in cross-sections for NC and CC cases (see **Figure 42** and **Figure 43**).

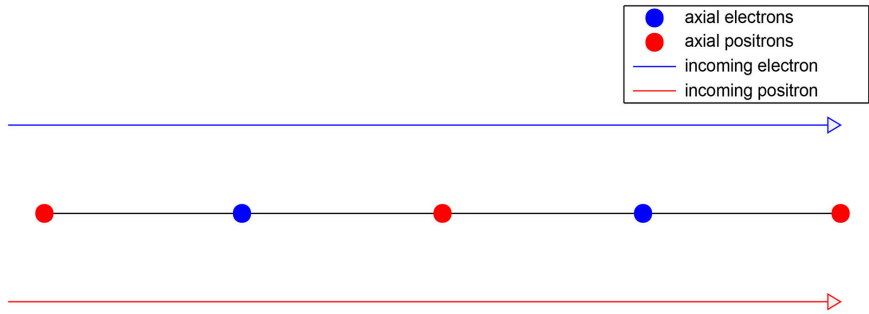


Figure 41. Picture showing why an electron has a larger scattering angle than a positron.

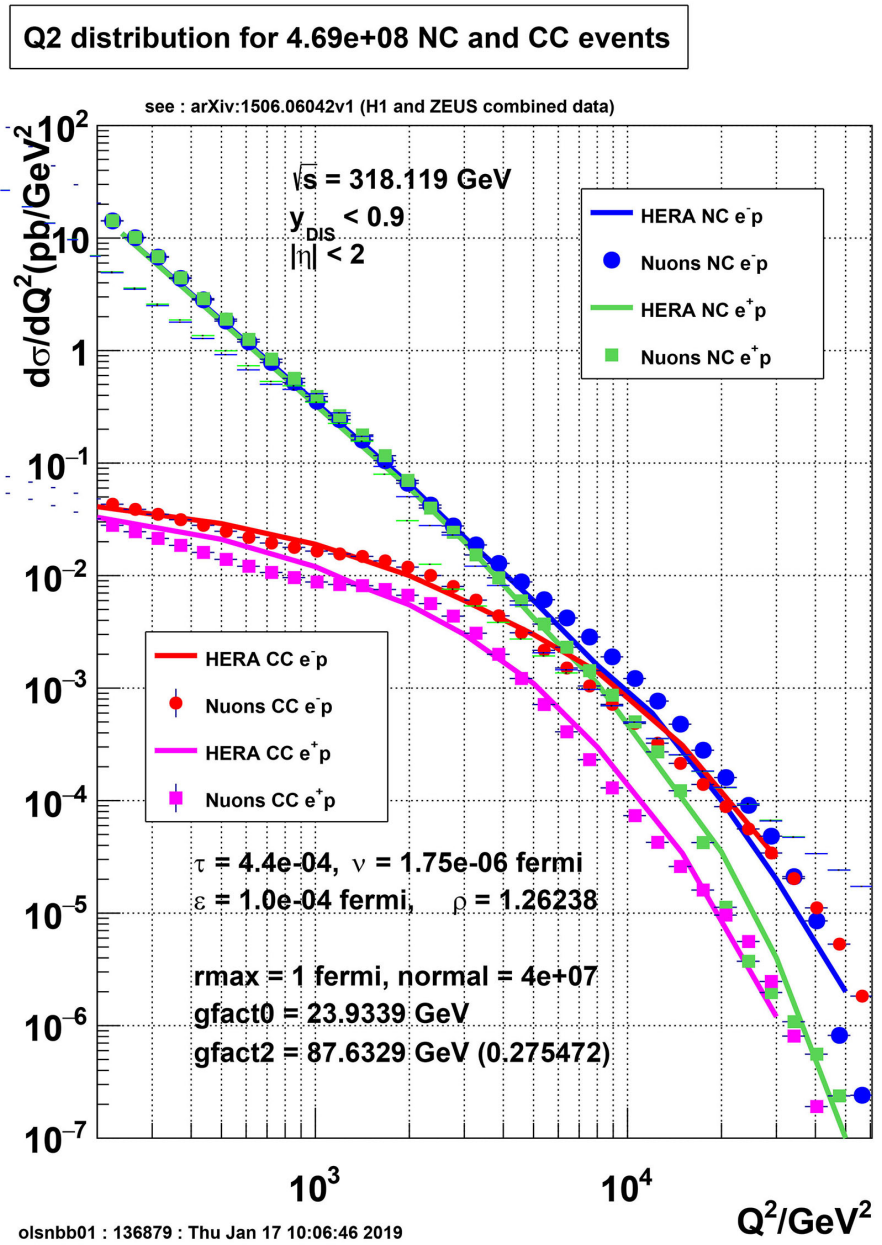


Figure 42. Q2 distribution for neutral and charged current events compared to HERA results.

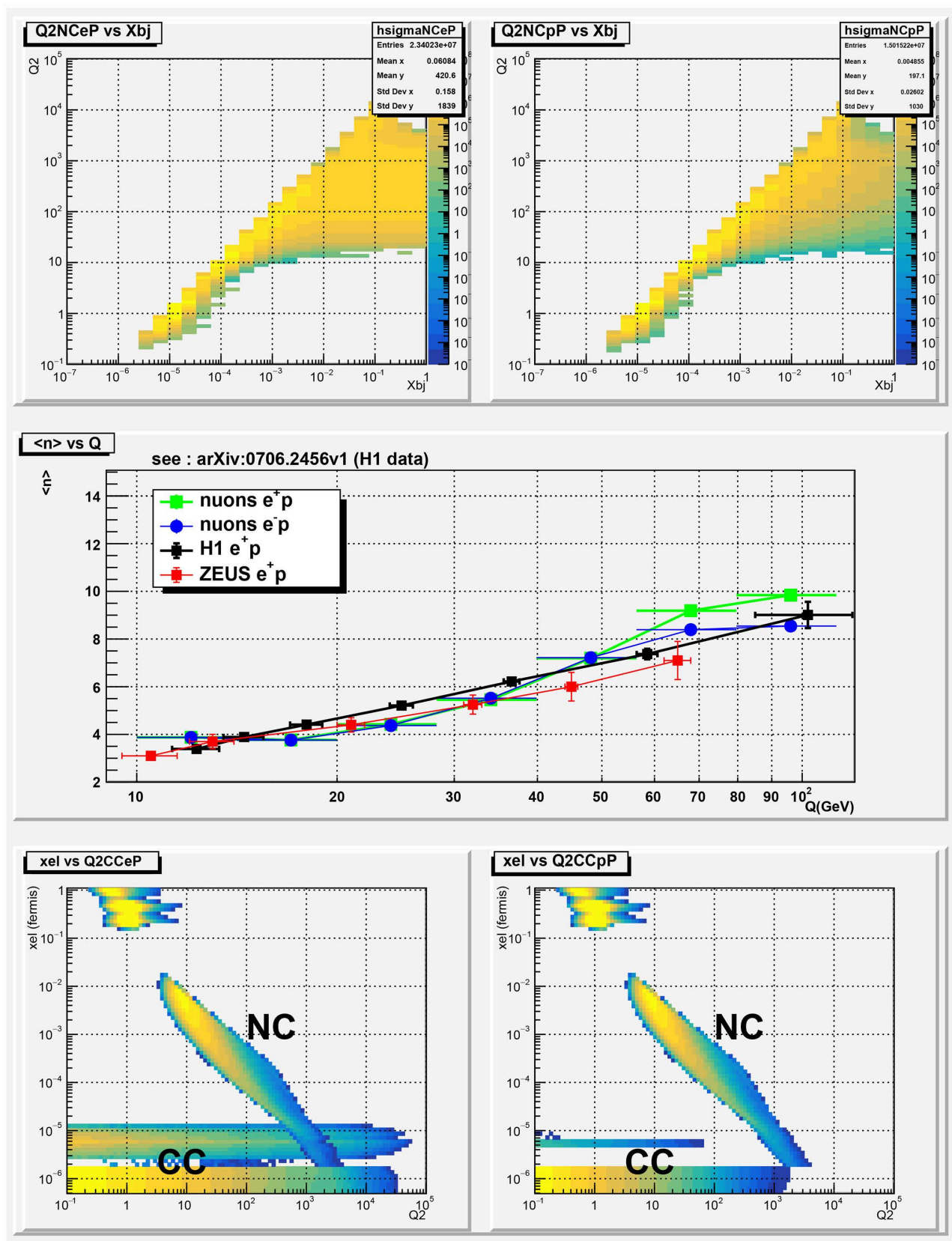


Figure 43. Top: Q^2 vs x for electron-proton (left) and positron-proton (right). Center: Average Charged particles multiplicity vs Q compared to HERA results. Bottom: Q^2 as a function of the distance (Fermi) electron-proton (left), or positron-proton (right).

It is fundamental for a better understanding of the central proton region to build as soon as possible new deep inelastic experiments to explore the center of mass energies ranging from 500 GeV to 5 TeV, and hence test all models up to a precision reaching the standard model quark or electron size.

11. Testing the Nuons Model with Heavy Ions Collisions

Two challenges were ahead to investigate these collisions:

Challenge 1: Which ion model? All experiments in this field use a theoretical model, typically the Glauber model to exploit the experimental data. This is somehow surprising, in particular when estimating the number of partners (colliding nucleons between the 2 ions). A model has been developed (see below) to build any ion (from deuterium to Uranium).

Challenge 2: Scarred by the CPU time necessary to make a collision? For instance the Lead ion with 82 proton and 126 neutrons, the nuons model has about $82 \times 66 + 126 \times 66$ nuons, about 13,728 nuons per ion, *i.e.* $4 \times 13,728 = 27,456$ electrons or positrons and as many neutrinos and antineutrinos per ion! This challenge was nearly unthinkable 10 years ago, but the advent of new powerful and not too expensive processors is now making this goal possible.

The program collidenuc has been developed to solve these 2 challenges. The ion is built by gradual insertion of nucleons around a central nucleon, respecting the ratio protons/neutrons and the distance between proton-proton, proton-neutron and neutron-neutron, each nucleon having a skin (0.09 fermi for proton and 0.01 fermi for neutron). These numbers are based on the computed electromagnetic forces between nucleons. The program assumes also an ellipsoidal shape for the nucleus. In the case of a Lead nucleus, the radius is around 6.5 fermi. Once each nucleus has been built, it is filled with electrons and positrons taken from a data base of protons and neutrons previously generated by the program findall.

To generate a collision between the 2 nuclei, a double loop is performed to check if one of the 27,456 electrons or positrons in each nucleus can collide following the distance rules already explained in the proton-proton collide program. **Figure 44** and **Figure 45** show various parameters compared with results from the Alice experiment at 5 TeV/nucleon: -Number of charged particles versus the centrality of the collision; -Number of collision partners (Npartners) versus centrality; -Charged particles divided by number Npartners versus centrality; -Charged particles divided by number Npartners versus Npartners.

The same results are available for ions collisions at 2760 GeV and 1000 GeV.

12. Nuons Are Possible Candidates for Dark Matter and Dark Energy

Nuons are expected to behave like heavy sterile neutrinos. They are continuously produced in proton-nucleon collisions within galaxies, supernova explosions, etc. As these nuons are rarely interacting, they are produced isotropic-ally. In a

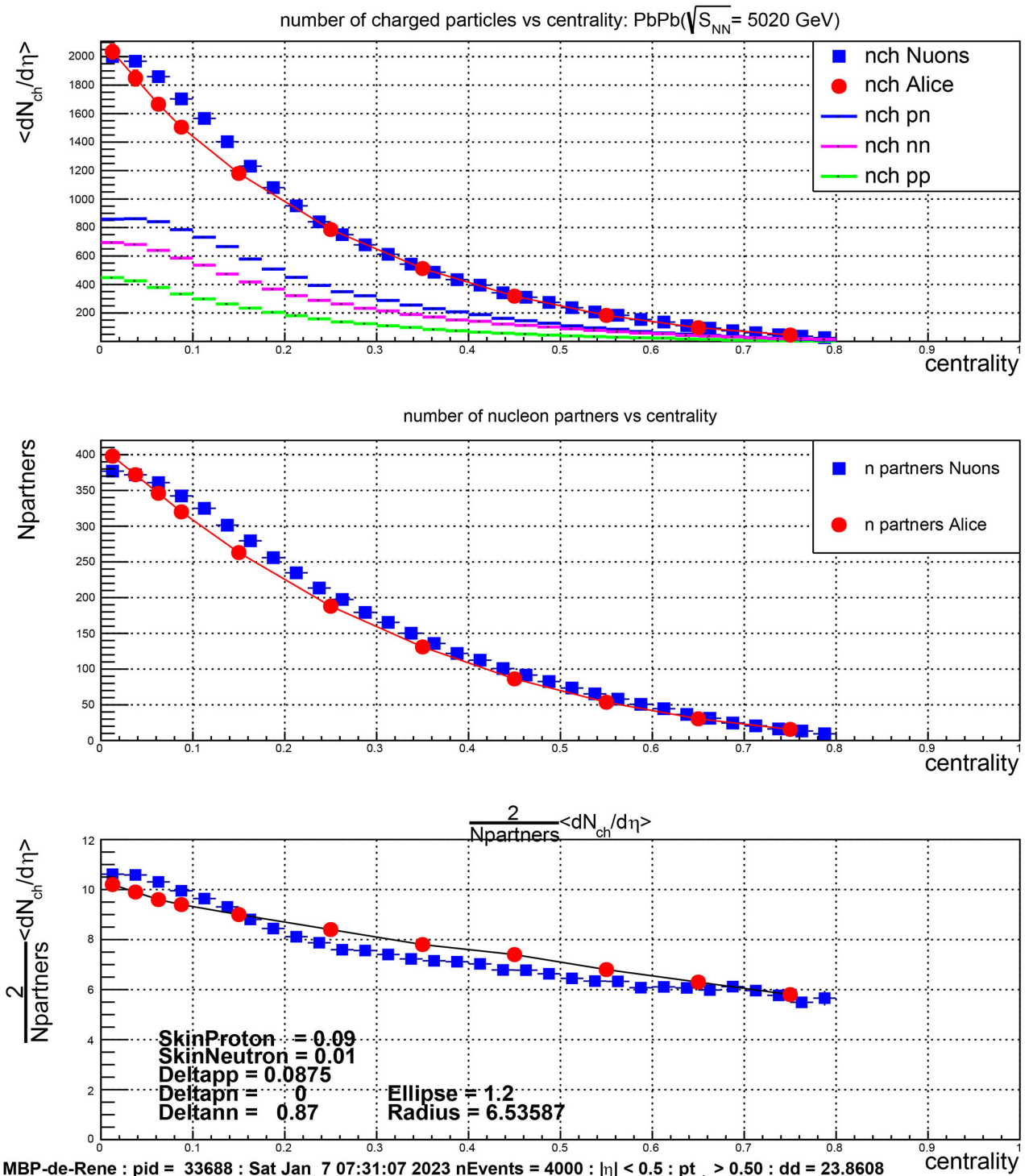


Figure 44. Top: Number of charged particles versus the centrality of the collision. Center: Number of collision partners (Npartners) versus centrality. Bottom: Charged particles divided by number Npartners versus centrality.

galaxy with a diameter of 1 million light years, they will happily fill the space between a galaxy and the surrounding galaxies after a few million years, adding a substantial amount of invisible matter to the galaxy. Recent results [34] confirm that the dark matter fills the space between galaxies in a uniform way. It would

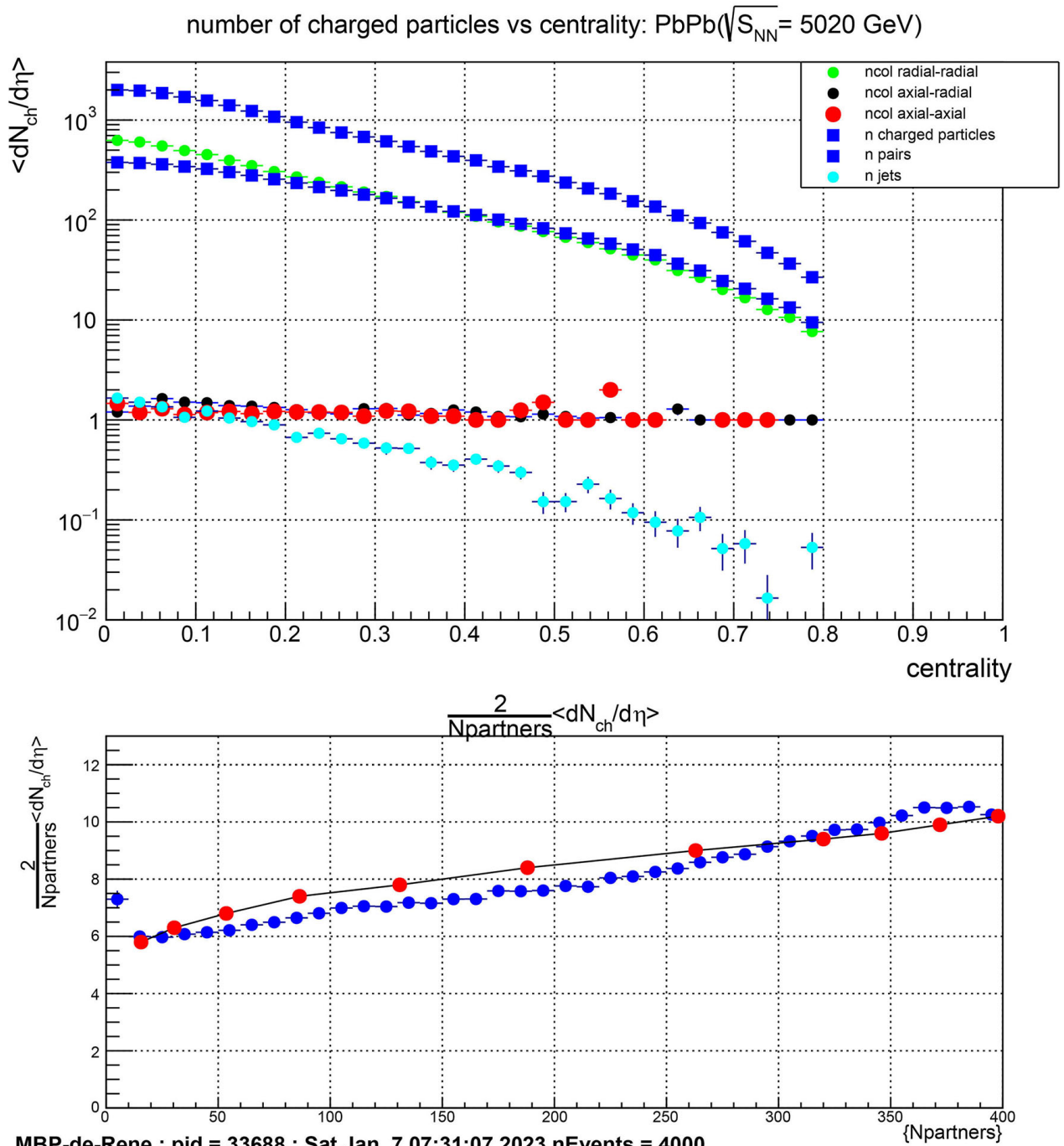


Figure 45. Top: Various types of collisions versus centrality. Bottom: Charged particles divided by number $N_{partners}$ versus $N_{partners}$.

be interesting to estimate the number of nuons produced per unit of time in a galaxy to find out if the sum of their masses can contribute to 25 percent of the mass of the galaxy. These nuons emitted in the collisions can go through all galaxies after billions of light years. A growing number of nuons escape the visible universe and contribute more and more to the expansion of the universe, thanks to the usual gravitational laws. Well! just a guess!

13. Summary

A new model is proposed to describe particles with masses ranging from the muon to the Upsilon. Thanks to the introduction of the nuon as a building block at this scale, the masses of these particles are computed at 1/1000 precision or better and a linearity is observed between the mass and the number of nuon constituents. Particles can be built taking into account only Coulomb interactions and without introducing a strong force.

The model has been tested against many experimental results. The momentum transfer distribution for proton-proton elastic scattering agrees extremely well with the TOTEM data over 7 orders of magnitude as well as with previous results at lower energies. It reproduces the P_T distributions at all the LHC energies over 15 orders of magnitude as well as the pseudo-rapidity distributions in the $-7 < \eta < 7$ range and the particles multiplicity. The jets cross-section and internal jets properties agree extremely well with the recent data from ATLAS and CMS.

The simulation of electrons or positrons colliding protons reproduces very well the recent combined results of H1 and ZEUS at HERA about deep inelastic scattering.

The nuon model has been tested successfully against the heavy ions collisions results from LHC/Alice or BNL.

Conflicts of Interest

The author declares no conflicts of interest regarding the publication of this paper.

References

- [1] Glashow, S.L. (1961) *Nuclear Physics*, **22**, 579-588.
[https://doi.org/10.1016/0029-5582\(61\)90469-2](https://doi.org/10.1016/0029-5582(61)90469-2)
- [2] Weinberg, S. (1967) *Physical Review Letters*, **19**, 1264-1266.
<https://doi.org/10.1103/PhysRevLett.19.1264>
- [3] Salam, A. and Svartholm, N. (1968) Elementary Particle Physics Relativistic Groups and Analyticity. In: Svartholm, N., Ed., *8th Nobel Symposium*, Almqvist and Wiksell, Stockholm, 367.
- [4] Englert, F. and Brout, R. (1964) *Physical Review Letters*, **13**, 321-323.
<https://doi.org/10.1103/PhysRevLett.13.321>
- [5] Higgs, P.W. (1964) *Physical Review Letters*, **13**, 508-509.
<https://doi.org/10.1103/PhysRevLett.13.508>
- [6] Guralnik, G.S., Hagen, C.R. and Kibble, T.W.B. (1964) *Physical Review Letters*, **13**, 585-587. <https://doi.org/10.1103/PhysRevLett.13.585>
- [7] Oerter, R. (2006) *The Theory of Almost Everything: The Standard Model, the Unsung Triumph of Modern Physics*. Plume, New York.
- [8] Schumm, B.A. (2004) *Deep Down Things: The Breathtaking Beauty of Particle Physics*. Johns Hopkins University Press, Baltimore.
- [9] Brun, R., *et al.* (1987) GEANT3: Detector Description and Simulation Tool. CERN

- Program Library Long Writeup W5013, Geneva. <https://cds.cern.ch/record/1119728>
- [10] Brun, R., *et al.* (1987) PAW—Physics Analysis Workstation. The Complete CERN Program Library. Version 1.07.
- [11] Brun, R. and Rademakers, F. (1997) *Nuclear Instruments and Methods in Physics Research Section A: Accelerators, Spectrometers, Detectors and Associated Equipment*, **389**, 81-86. [https://doi.org/10.1016/S0168-9002\(97\)00048-X](https://doi.org/10.1016/S0168-9002(97)00048-X)
- [12] Durr, S., *et al.* (2008) *Science*, **322**, 1224-1227. <https://doi.org/10.1126/science.1163233>
- [13] Antchev, G., *et al.* (2011) *Europhysics Letters*, **95**, 41001.
- [14] H1 and ZEUS Collaborations (2015) Combination of Measurements of Inclusive Deep Inelastic e + -p Scattering Cross Sections and QCD Analysis of HERA Data.
- [15] James, F. (1988) MINUIT—Interpretation of the Errors on Parameters. CERN Program Library D506 Supplement.
- [16] PDG. Particles Data Group, Data Taken from Review of Particle Physics. https://pdg.lbl.gov/2020/tables/contents_tables_mesons.html
- [17] Koide, Y. (1983) *Physics Letters B*, **120**, 161.
- [18] Greulich, K.O. (2010) *Journal of Modern Physics*, **1**, 300-302. <https://doi.org/10.4236/jmp.2010.15042>
- [19] Paasch, K. (2017) On the Calculation of Elementary Particle Masses. <https://hal.archives-ouvertes.fr/hal-01368054v3>
- [20] Smith, T.P. (2010) *Nature*, **98**, 478-485.
- [21] Nagy, E., *et al.* (1979) *Nuclear Physics B*, **150**, 221-267. [https://doi.org/10.1016/0550-3213\(79\)90301-8](https://doi.org/10.1016/0550-3213(79)90301-8)
- [22] Nachtmann, O. (2003) Pomeron Physics and QCD.
- [23] Collins, P.D.B. (1977) An Introduction to Regge Theory and High-Energy Physics. Cambridge University Press, Cambridge. <https://doi.org/10.1017/CBO9780511897603>
- [24] UA4 Collaboration (1985) *Physics Letters B*, **155**, 197-202. [https://doi.org/10.1016/0370-2693\(85\)90985-2](https://doi.org/10.1016/0370-2693(85)90985-2)
- [25] D0 Collaboration (2010) Soft QCD Results from D0. <https://arxiv.org/ftp/archiv/papers/1011/1011.6360.pdf>
- [26] The CMS Collaboration (2011) Charged Particle Transverse Momentum Spectra in pp Collisions at $\sqrt{s} = 0.9$ and 7 TeV.
- [27] Mateos, D.L. (2011) Measurement of Multi-JET Production Cross Section at a Center-of-Mass Energy of 7 TeV at the Large Hadron Collider with the Atlas Detector. Thesis, CERN-THESIS-2011-039.
- [28] The ALICE Collaboration (2010) Transverse Momentum Spectra of Charged Particles in Proton-Proton Collisions at $\sqrt{s} = 900$ GeV.
- [29] Shlyapnikov, P.V. (1992) *Uspekhi Fizicheskikh Nauk*, **162**, 1-28. <https://doi.org/10.3367/UFNr.0162.199206a.0001>
- [30] The ALICE Collaboration (2012) Transverse Sphericity of Primary Charged Particles in Minimum Bias Proton-Proton Collisions at $\sqrt{s} = 0.9, 2.76$ and 7 TeV. CERN-PH-EP-2010-010, May.
- [31] CMS Collaboration (2013) Jet and Underlying Event Properties as a Function of Particle Multiplicity in Proton-Proton Collisions at $\sqrt{s} = 7$ TeV. CERN-PH-EP/2013-195.

- [32] The ATLAS Collaboration (2011) *European Physical Journal C*, **71**, Article No. 1763.
- [33] CMS Collaboration (2014) Charged Jet Cross Sections and Properties in Proton-Proton Collisions at $\sqrt{s} = 7$ TeV. CERN-PH-EP/2014-254.
- [34] Masaki, S., Fukugita, M. and Yoshida, N. (2012) *The Astrophysical Journal*, **746**, 38. <https://doi.org/10.1088/0004-637X/746/1/38>